

# 1 Clickable Shiga Toxin B Subunit for Drug Delivery in Cancer Therapy

2 Natalia Danielewicz,<sup>¶</sup> Francesca Rosato,<sup>¶</sup> Jana Tomisch, Jonas Gräber, Birgit Wiltschi, Gerald Striedner,  
3 Winfried Römer, and Juergen Mairhofer<sup>\*†</sup>

 Cite This: <https://doi.org/10.1021/acsomega.3c00667>

 Read Online

ACCESS |

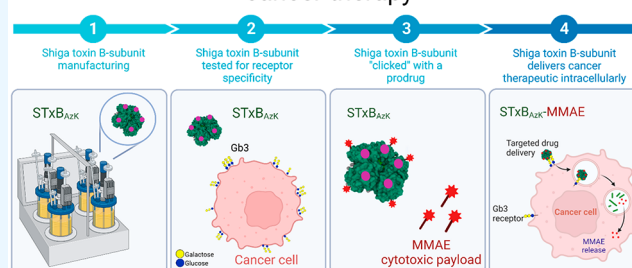
 Metrics & More

 Article Recommendations

 Supporting Information

4 **ABSTRACT:** In recent years, receptor-mediated drug delivery has  
5 gained major attention in the treatment of cancer. The pathogen-  
6 derived Shiga Toxin B subunit (STxB) can be used as a carrier that  
7 detects the tumor-associated glycosphingolipid globotriaosylcer-  
8 amide (Gb3) receptors. While drug conjugation via lysine or  
9 cysteine offers random drug attachment to carriers, click chemistry  
10 has the potential to improve the engineering of delivery systems as  
11 the site specificity can eliminate interference with the active  
12 binding site of tumor ligands. We present the production of  
13 recombinant STxB in its wild-type (STxB<sub>wt</sub>) version or  
14 incorporating the noncanonical amino acid azido lysine (STxB<sub>AzK</sub>).  
15 The STxB<sub>wt</sub> and STxB<sub>AzK</sub> were manufactured using a growth-  
16 decoupled *Escherichia coli* (*E. coli*)-based expression strain and analyzed via flow cytometry for Gb3 receptor recognition and  
17 specificity on two human colorectal adenocarcinoma cell lines—HT-29 and LS-174—characterized by high and low Gb3  
18 abundance, respectively. Furthermore, STxB<sub>AzK</sub> was clicked to the antineoplastic agent monomethyl auristatin E (MMAE) and  
19 evaluated in cell-killing assays for its ability to deliver the drug to Gb3-expressing tumor cells. The STxB<sub>AzK</sub>–MMAE conjugate  
20 induced uptake and release of the MMAE drug in Gb3-positive tumor cells, reaching 94% of HT-29 cell elimination at 72 h post-  
21 treatment and low nanomolar doses while sparing LS-174 cells. STxB<sub>AzK</sub> is therefore presented as a well-functioning drug carrier,  
22 with a possible application in cancer therapy. This research demonstrates the feasibility of lectin carriers used in delivering drugs to  
23 tumor cells, with prospects for improved cancer therapy in terms of straightforward drug attachment and effective cancer cell  
24 elimination.

## Clickable Shiga toxin B-subunit for drug delivery in cancer therapy



25 **T**he improvement of strategies for targeted drug delivery  
26 has gained importance in multiple fields, e.g., vaccinology,  
27 neurology, gene therapy, and cancer treatment.<sup>1–3</sup> A drawback  
28 of classically administered therapeutics is their limited  
29 capability to navigate across biological barriers to finally  
30 reach the intended site of action. Overcoming patient's  
31 heterogeneity has been accomplished through precision  
32 therapeutics, in which the active pharmaceutical ingredient  
33 (API) can be coupled to a carrier capable of recognizing and  
34 targeting the cells and tissues of interest with high selectivity  
35 (Figure 1). This approach has been investigated to enhance the  
36 therapeutic efficacy of treatments by concentrating them at the  
37 desired site of action, thus limiting the side effects and dose-  
38 related toxicity of a systemic administration. Several new  
39 anticancer treatments have shown promising efficacy by  
40 exploiting ligands of membrane receptors as selective carriers  
41 for a toxic payload.<sup>4,5</sup> Among the most successful drug delivery  
42 systems, several antibody–drug conjugates (ADCs), such as  
43 Brentuximab Vedotin (cAC10-vcMMAE, SGN-35), have made  
44 their appearance on the market and improved the outcome of  
45 tumor therapies.<sup>6–8</sup>

46 The design of an appropriate API delivery system relies,  
47 among others, on the type of receptor to be targeted by the

carrier of the drug. As such, certain carbohydrate-binding 48  
proteins, which recognize sugar moieties attached to proteins 49  
and lipids on cell surfaces, offer a wide range of opportunities 50  
for the development of carrier-based drug delivery in modern 51  
medicine. For example, Shiga Toxin (STx) provides a means 52  
for developing novel cancer treatments.<sup>9,10</sup> The STx complex, 53  
which is composed of a toxic catalytic A subunit and a 54  
pentamer of nontoxic receptor-binding B subunits, has been an 55  
effective tool in various therapeutic approaches, including 56  
tumor treatment and imaging.<sup>11</sup> If expressed recombinantly 57  
without the A subunit, the B subunits are referred to as STxB. 58  
STxB is a multipurpose protein applicable, for example, to 59  
tumor targeting and vaccine design. Each application is 60  
determined by the presence of its preferential receptor, the 61  
glycosphingolipid (GSL) globotriaosylceramide (Gb3, also 62  
known as CD77 or P<sup>k</sup> antigen) on target cells. Upon binding to 63

Received: February 1, 2023

Accepted: March 10, 2023

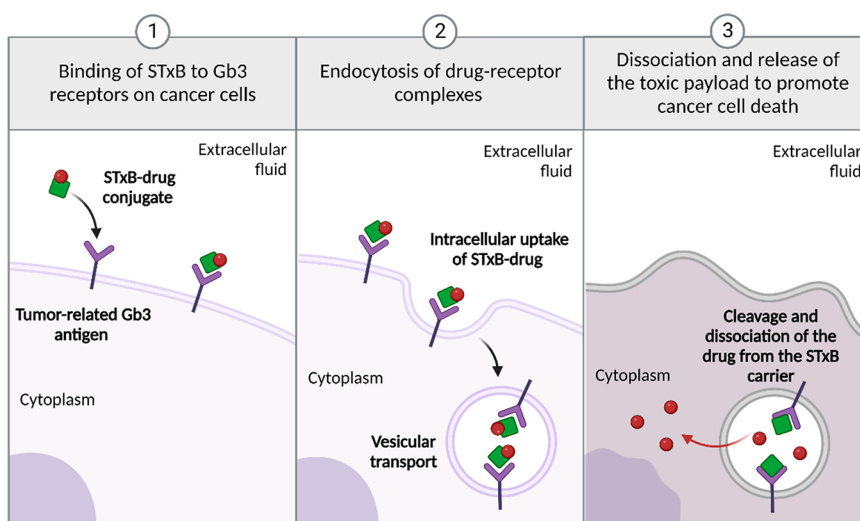


**Figure 1.** Internalization of Shiga Toxin B subunit (STxB) enabling a method for drug delivery. Created with BioRender.com.

64 Gb3 at the plasma membrane, STxB is internalized by  
65 endocytosis and can be found in clathrin-coated pits.<sup>12</sup>  
66 Alternatively, when clathrin-dependent uptake is blocked,  
67 STxB endocytosis continues via the clathrin-independent  
68 pathway, without the help of the cytosolic machinery. STxB  
69 can induce the formation of the STxB-Gb3 cluster domains,  
70 imposing negative curvature on the host membrane and  
71 promoting lipid reorganization in tubular membrane invagina-  
72 tions.<sup>13,14</sup> These events ultimately lead to STxB entry in the  
73 intracellular space and its retrograde transport from early  
74 endosomes to the *trans*-Golgi network and the endoplasmic  
75 reticulum (ER).<sup>15,16</sup> STxB has been described as a well-  
76 performing API carrier if modified via random *N*-hydrox-  
77 ysuccinimide (NHS)–biotin coupling and maleimide chem-  
78 istry or expressed recombinantly with other fusion proteins and  
79 as such enables the delivery of small molecules, modified  
80 proteins, or nanoparticles (Figure 1).<sup>17,18</sup> Such methods,  
81 however, often require time-consuming optimization experi-  
82 ments, resulting in high batch-to-batch variability, and  
83 extensive losses during purification. Alternatively, the site-  
84 specific incorporation of reactive noncanonical amino acids  
85 (ncAAs) like *L*-azido lysine (AzK, *N*6-((2-azidoethoxy)-  
86 carbonyl)-*L*-lysine) can be used to overcome the above-  
87 mentioned problems and reach higher efficiency of STxB–drug  
88 conjugation.<sup>19</sup> This approach can be advanced even further if  
89 combined with controlled decoupling of recombinant protein  
90 production from cell growth to considerably increase the ncAA  
91 incorporation.<sup>20</sup> The enGenes-X-press *E. coli* strains have  
92 previously proven to be successful in the production of  
93 homologous cholera toxins.<sup>21</sup>

94 To investigate the efficiency of the selected carrier STxB in  
95 drug delivery, the choice of a model drug also plays a crucial  
96 role. The most straightforward approach is the selection of  
97 previously tested small molecules that are equipped with a  
98 cleavable linker. An example of such a drug is DBCO-PEG4-  
99 Val-Cit-PAB-MMAE, a toxic payload composed of (I) a potent  
100 tubulin polymerization inhibitor, monomethyl auristatin E  
101 (MMAE), (II) a reactive dibenzocyclooctyne group (DBCO)  
102 that allows copper-free click chemistry to azide groups (–N<sub>3</sub>;  
103 AzK), (III) distanced by a four-unit polyethylene glycol  
104 (PEG), and (IV) an enzymatically cleavable linker (Val-Cit-  
105 PAB). The peptide bond between Cit-PAB of dipeptide linkers

containing valine (Val)-citrulline (Cit) and *p*-amino benzyl 106  
alcohol (PAB) is cleaved by a ubiquitous cysteine protease, the 107  
cathepsin B, which is located in late endosomes and 108  
lysosomes.<sup>22–24</sup> The linker between the cytotoxic drug and 109  
the carrier is a critical part of the design of a carrier–drug 110  
conjugate, as it must retain stability in the circulation and 111  
prevent nonspecific drug release while enabling the detach- 112  
ment of the drug at the site of action.<sup>25,26</sup> The DBCO-PEG4- 113  
Val-Cit-PAB-MMAE delivered to lysosomes is cleaved off as 114  
PAB-MMAE and released to the cytosol, resulting in mitotic 115  
arrest and apoptosis.<sup>27</sup> DBCO-PEG4-Val-Cit-PAB-MMAE has 116  
been used for the synthesis of antibody–drug conjugates 117  
(ADCs).<sup>28–31</sup> Similar approaches were further proven 118  
successful in the literature.<sup>19,32</sup> 119

Antibodies generally differ as carriers of drugs from STxB by 120  
following mainly the lysosomal pathway.<sup>9</sup> STxB is rapidly 121  
internalized into target cells by endocytosis,<sup>12,13</sup> and its 122  
intracellular sorting is directed by the presence of Gb3 in 123  
lipid rafts. Lipid rafts are dynamic membrane microdomains 124  
enriched in sphingomyelin and cholesterol.<sup>33</sup> When bound to 125  
nonlipid raft Gb3, STxB follows the degradative pathway to 126  
lysosomes.<sup>34,35</sup> This fraction of lysosomal STxB offers an 127  
opportunity for the targeted intracellular delivery of drugs such 128  
as DBCO-PEG4-Val-Cit-PAB-MMAE. The delivery of anti- 129  
tumoral drugs by STxB was previously tested on Gb3- 130  
expressing tumor cell lines derived from colorectal, lung, or 131  
breast carcinomas.<sup>36–41</sup> These human cell lines are an effective 132  
model for assessing the ability of STxB to deliver various 133  
treatments *in vitro*. 134

Here, we tested our products for purity, activity, and 135  
intracellular uptake in the Gb3-positive (Gb3<sup>+</sup>) human 136  
colorectal adenocarcinoma cell line HT-29. The specificity of 137  
generated STxB variants was further monitored on the LS-174 138  
cell line, derived from human colon adenocarcinoma as well 139  
but characterized by a low Gb3 abundance.<sup>42</sup> We customized 140  
the STxB carrier with reactive bioorthogonal (“click”) handles 141  
by the site-specific incorporation of the reactive ncAA AzK. 142  
The AzK residue was incorporated in the STxB sequence 143  
following three primary requirements: (i) incorporation of the 144  
ncAA should occur at the surface of the protein; (ii) the ncAA 145  
should be inserted at a distance from the receptor binding site, 146  
to avoid interference with the binding; and (iii) the residues in 147

148 the pentameric structure should be located at a distance from  
149 each other to facilitate their derivatization with the API. In the  
150 STxB amino acid sequence, the K9 residue, oriented such that  
151 it opposes the Gb3-binding pockets facing the membrane, was  
152 chosen to fulfill these conditions. The azido-functionalized  
153 proteins are cross-linked by linker molecules carrying  
154 compatible reactive groups for click chemistry, such as  
155 DBCO. The nontoxic STxB<sub>wt/AzK</sub> variants were produced  
156 using the growth-decoupled *E. coli* enGenes-X-press sys-  
157 tem<sup>20,21,43</sup> equipped with an orthogonal aminoacyl-tRNA  
158 synthetase/amber suppressor tRNA pair,<sup>20</sup> which allows for  
159 site-specific ncAA incorporation. The goal is to enable the  
160 production of well-defined, site-specifically labeled API carriers  
161 to be used for targeted drug delivery in a model *in vitro* setup  
162 in which DBCO-PEG4-Val-Cit-PAB-MMAE represents the  
163 drug of choice.

## 164 ■ MATERIAL AND METHODS

165 **Antibodies and Chemicals.** The following antibodies  
166 were used: Alexa Fluor 647-labeled anti-6-His epitope tag  
167 (Cat. No. 362611) from BioLegend (San Diego, CA, USA),  
168 Anti-Giantin mouse monoclonal antibody (Cat. No. ab37266)  
169 purchased from Abcam (Waltham, Boston, USA), LAMP1  
170 (D2D11) XP rabbit monoclonal antibody (Cat. No. 9091)  
171 obtained from Cell Signaling Technology (Danvers, Massa-  
172 chusetts, USA), and Cy3-AffiniPure F(ab')<sub>2</sub> Fragment Donkey  
173 Anti-Rabbit IgG (H+L) polyclonal antibody (Cat. No. 711-  
174 166-152) and Cy3-AffiniPure Donkey Anti-Mouse IgG (H+L)  
175 polyclonal antibody (Cat. No. 715-165-150) supplied by  
176 Jackson ImmunoResearch (West Grove, Pennsylvania, USA).  
177 The following reagents were obtained from commercial  
178 sources: PBS, FBS, HEPES, NEAA, and 0.05% Trypsin-  
179 EDTA (1x) were purchased from Gibco (Thermo Fisher  
180 Scientific Inc., Rockford, IL, USA). DMSO, penicillin/  
181 streptomycin, BSA, DAPI, glycerol, methanol, Triton X-100,  
182 and sodium hydrogen carbonate were obtained from Carl Roth  
183 GmbH & Co. KG (Karlsruhe, Baden-Württemberg, Germany).  
184 D-Luciferin Firefly was provided by Biosynth (Staad, Switzer-  
185 land), and DMEM (with: 1.0 g/L of glucose, stable glutamine,  
186 sodium pyruvate, 3.7 g/L of NaHCO<sub>3</sub>) was purchased from  
187 PAN Biotech (Aidenbach, Bayern, Germany). DL-Threo-1-  
188 phenyl-2-palmitoylamino-3-morpholino-1-propanol (PPMP)  
189 was obtained from Sigma-Aldrich Chemie GmbH (Saint  
190 Louis, MO, USA).

191 **STxB<sub>wt/AzK</sub> Construct Design.** The amino acid sequence  
192 of STxB<sub>wt</sub> protein with a fused C-terminal 6x His-tag was  
193 subcloned into pET30a-Cer and<sup>21</sup> and pSCS-T7 × 31<sup>28</sup>, and  
194 STxB<sub>AzK</sub> including a C-terminal 6x His-tag with a mutation on  
195 position Lys9 in pSCS\_T7 × 31 (Supporting Information  
196 Figure 1) was used for expression.<sup>44</sup> The three plasmids were  
197 named pET30a<STxB<sub>wt</sub>>Cer, pSCS-T7 × 31<STxB<sub>wt</sub>>, and  
198 pSCS-T7 × 31<STxB<sub>AzK</sub>>. All materials used for cloning were  
199 purchased from New England Biolabs, Frankfurt, Germany  
200 (cloning kits), and IDT, Leuven, Belgium (primers and  
201 gBLOCKs).

202 **STxB<sub>wt/AzK</sub> Expression, Purification, and Off-Line**  
203 **Analytcs.** The expression of all constructs was carried out  
204 in the BL21(DE3) strain and enGenes-X-press strain, called  
205 V1,<sup>21</sup> originating from BL21(DE3). For  $\mu$ -bioreactor culti-  
206 vations, we used the  $\mu$ -bioreactor Biolector system, Beckmann  
207 Coulter, Germany, and for benchtop fed-batch cultures the  
208 Dasgip Parallel Bioreactor System, Eppendorf, Germany.  
209 Media composition and standard cultivation protocols are

described in ref 21. The full-to-low induction strategy was  
210 implemented with IPTG (0.5–0.01 mM; GERBU Biotechnik,  
211 Heidelberg, Germany) and/or L-arabinose (100 mM; Sigma-  
212 Aldrich, A3256, Saint Louis, Missouri, USA). Arabinose (Ara)  
213 was only added to the V1 strain as described in ref 21. Five  
214 mM of AzK (Iris Biotech, Marktredwitz, Germany) was added  
215 to the  $\mu$ -bioreactor at the start of culture and to the benchtop  
216 bioreactor at the start of feed for strains cultivated for STxB<sub>AzK</sub>  
217 production (both V1 and BL21 (DE3)). All  $\mu$ -scale cultures  
218 were run over 24 h. An amount of 1 mg of cell dry mass  
219 (CDM) was harvested and enzymatically lysed, and the  
220 product yield was analyzed.<sup>45</sup> The results from  $\mu$ -scale  
221 cultivation were translated to a large scale (benchtop 1 L),  
222 and the V1 strain was cultivated to 37 g/L of final CDM. For  
223 STxB<sub>wt</sub> production, two different induction strategies were  
224 implemented. The first conventional one was direct pulse  
225 induction (0.5 mM IPTG + 100 mM Ara). The second  
226 optimized fermentation was a combination of pulse and feed  
227 induction calculated to the final volume, called low induction  
228 (0.01 mM IPTG + 100 mM Ara), partial induction (0.1 mM  
229 IPTG + 100 mM Ara), and full induction/low induction (0.5  
230 mM IPTG + 100 mM Ara). For STxB<sub>AzK</sub>, the full induction  
231 condition was supplemented with 5 mM AzK.<sup>44</sup> For all  
232 benchtop cultivations, cells were harvested at the end of  
233 fermentation and resuspended in 50 mM Na<sub>2</sub>HPO<sub>4</sub>/  
234 NaH<sub>2</sub>PO<sub>4</sub>, 500 mM NaCl, and 20 mM imidazole (Sigma-  
235 Aldrich, Saint Louis, Missouri, USA) at pH 7.4 to yield a 30 g  
236 CD mg/L suspension. The suspension was homogenized at  
237 700/70 (first stage/second stage) bar for 2 passages on a GEA  
238 Niro Soavi PANDAPlus 2000 (GEA, Parma, Italy). Removal of  
239 cell debris was achieved by centrifugation and a filtration step  
240 on a 0.2  $\mu$ m sterile filter (Fluorodyne EX EDF, Pall  
241 Corporation, Dreieich, Germany). A two-step purification  
242 was performed by ÄKTA start (Cytiva, Uppsala, Sweden),  
243 starting with HisTrap FF (5 mL) (Cytiva, Uppsala, Sweden)  
244 with an immobilized metal affinity chromatography (IMAC)  
245 Cytiva protocol followed by size exclusion chromatography  
246 (SEC) Superdex 75 10/300 GL with ÄKTA PURE (Cytiva,  
247 Uppsala, Sweden). The binding/wash buffer for each  
248 purification was: 50 mM Na<sub>2</sub>HPO<sub>4</sub>/NaH<sub>2</sub>PO<sub>4</sub>, 500 mM  
249 NaCl, and 20 mM Imidazole pH 7.4. The product purified  
250 with HisTrap FF was eluted with a binding buffer  
251 supplemented with 300 mM imidazole (Sigma-Aldrich,  
252 S6749, Vienna, Austria). The SEC purification buffer was  
253 phosphate-buffered saline (PBS). The final product was  
254 rebuffed in Dulbecco's phosphate-buffered saline buffer  
255 (DPBS) (PANtm Biotech, Aidenbach, Germany) using  
256 Amicon Ultra Centrifugal Filters (30 kDa cutoff; Darmstadt,  
257 Germany).  
258

All off-line analytics like SDS-PAGE and analytical SEC  
259 coupled with multiangle light scattering (MALS) were  
260 performed as described in ref 21. The molecular weight of  
261 the constructs was analyzed by SEC, coupled with right-angle  
262 light scattering (RALS), using an OMNISEC RESOLVE/  
263 REVEAL combined system (Malvern Panalytical, Malvern,  
264 UK). The MS analysis was conducted by directly injecting  
265 STxB<sub>AzK</sub>-MMAE into an LC-ESI-MS system (LC: Agilent  
266 1290 Infinity II UPLC, SA, USA). A gradient from 15 to 80%  
267 acetonitrile in 0.1% formic acid (using a Waters BioResolve  
268 column (2.1 × 5 mm); Vienna, Austria) at a flow rate of 400  
269  $\mu$ L/min was applied (9 min gradient time). Detection was  
270 performed with a Q-TOF instrument (Agilent Series 6230 LC-  
271 TOFMS, SA, USA) equipped with the Jetstream ESI source in

273 positive ion, MS mode (range: 400–3000 Da). Instrument  
274 calibration was performed using an ESI calibration mixture  
275 (Agilent). Data were processed using MassHunter BioConfirm  
276 B.08.00 (Agilent), and the spectrum was deconvoluted by  
277 MaxEnt.

278 **STxB<sub>wt/AzK</sub> Labeling.** For cell-based assays, STxB<sub>wt</sub> and  
279 STxB<sub>AzK</sub> were fluorescently labeled with commercially available  
280 dyes. For the initial assessment of Gb3 abundance at the  
281 surface of treated cells, commercial STxB (Sigma-Aldrich  
282 Chemie GmbH, Germany) was dissolved at 1 mg/mL in PBS  
283 and stored at 4 °C prior to its use. For fluorescence labeling,  
284 Cy5 monoreactive NHS ester (GE Healthcare, Boston, MA,  
285 USA) was used. The fluorescent dye was dissolved at a final  
286 concentration of 10 mg/mL in water-free DMSO, aliquoted,  
287 and stored at –20 °C before usage according to the  
288 manufacturer's protocol. For fluorescence labeling of STxB<sub>wt</sub>  
289 produced in this study, AlexaFluor 647 NHS ester (Thermo  
290 Fisher Scientific Inc., Massachusetts, USA) was used. The  
291 fluorescent dye was dissolved at a final concentration of 10  
292 mg/mL in water-free DMSO (Carl Roth GmbH & Co. KG,  
293 Baden-Württemberg, Germany), aliquoted, and stored at –20  
294 °C before usage according to the manufacturer's protocol. For  
295 the labeling reactions, 100 μL of STxB or STxB<sub>wt</sub> (18 μM) was  
296 supplemented with 10 μL of a 1 M NaHCO<sub>3</sub> (pH 9) solution  
297 so that the molar ratio between dye and STxB was 6:1. The  
298 labeling mixture was incubated at 25 °C for 60 min under  
299 continuous stirring, and uncoupled dye was removed using  
300 Zeba Spin desalting columns (7 kDa MWCO, 0.5 mL, Thermo  
301 Fisher Inc., Rockford, IL, USA). Cy5-labeled STxB and AF647-  
302 labeled STxB<sub>wt</sub> were stored at 4 °C and protected from light.  
303 STxB<sub>AzK</sub> (21 μM) was mixed with a ten-times excess of  
304 DBCO-AF647 (Jena Bioscience GmbH, Thuringia, Germany)  
305 in a total volume of 50 μL in PBS at 22 °C and incubated with  
306 shaking at 600 rpm overnight in the dark. 5x SDS reducing  
307 buffer was added directly to the sample to stop the reaction.  
308 Subsequently, uncoupled dyes were removed using Zeba Spin  
309 desalting columns (7 kDa MWCO, 0.5 mL, Thermo Fisher  
310 Inc., Rockford, IL, USA). AF647-labeled STxB<sub>AzK</sub> was stored at  
311 4 °C in the absence of light.

312 **Conjugation of STxB<sub>AzK</sub> and DBCO-PEG4-Val-Cit-PAB-  
313 MMAE.** The DBCO-PEG4-Val-Cit-PAB-MMAE from Broad-  
314 pharm (San Diego, CA, USA) was dissolved in DMSO (Carl  
315 Roth GmbH & Co. KG, Baden-Württemberg, Germany) to a  
316 final concentration of 5 mM and stored at –20 °C in the dark  
317 until use. Cu-free click chemistry (SPAAC) was performed for  
318 16 h at RT in 100 μL of PBS (pH 7.4) containing 21 μM  
319 STxB<sub>AzK</sub> and DBCO-PEG4-Val-Cit-PAB-MMAE at different  
320 molar ratios, i.e., 1:5, 1:10, or 1:20. The DMSO concentration  
321 was maintained between 8 and 10% (v/v) in the reaction  
322 mixtures. To terminate the reaction and remove the unreacted  
323 DBCO-PEG4-Val-Cit-PAB-MMAE, 5x SDS reducing buffer  
324 was added directly to the reaction mixtures, and the samples  
325 were buffer-exchanged with PBS (pH 7.4) using Zeba Spin  
326 desalting columns (7 kDa MWCO, 0.5 mL, Thermo Fisher  
327 Inc., Rockford, IL, USA). The concentration of the three  
328 STxB<sub>AzK</sub>-MMAE conjugates (1:5, 1:10, and 1:20) was  
329 measured spectrophotometrically, and the solutions were  
330 stored at 4 °C until further use.

331 **Cell Lines.** Luciferase-expressing HT-29 and LS-174 human  
332 colon adenocarcinoma cell lines (kindly provided by PD Dr.  
333 Susana Minguet, Institut für Biologie III, Albert-Ludwigs  
334 Universität Freiburg, Germany) were used in this study. Both  
335 cell lines were cultured in Dulbecco's Modified Eagle's

Medium (DMEM) (with: 1.0 g/L of glucose, stable glutamine, 336  
sodium pyruvate, 3.7 g/L of NaHCO<sub>3</sub>) supplemented with 337  
10% (v/v) heat-inactivated fetal bovine serum (FBS), 2.5 μg/  
338 mL of penicillin/streptomycin, 1% (v/v) nonessential amino  
339 acids (ncAAs), and 1% (v/v) HEPES, in a humidified  
340 incubator with 5% CO<sub>2</sub> at 37 °C. If not stated differently, all  
341 experiments were performed in the described complete media. 342

**Depletion of Glucosylceramide-Based Glycosphingo-  
343 lipids by PMP Treatment.** To deplete HT-29 cells of 344  
globotriaosylceramide, 2 × 10<sup>5</sup> cells were seeded in 6-well 345  
plates and cultured for 72 h in the presence of 2 μM DL-threo- 346  
1-phenyl-2-palmitoylamino-3-morpholino-1-propanol 347  
(PMP), an inhibitor of the synthesis of glucosylceramide- 348  
based GSLs.<sup>46</sup> Depletion of Gb3 from the plasma membrane of 349  
treated cells was assessed by flow cytometry analysis by using 350  
2.6 nM STxB<sub>wt</sub> AF647 and STxB<sub>AzK</sub> AF647 in binding assays. 351

**Ligand- and Cell-Based Binding Assays.** The binding of 352  
Gb3 to STxB<sub>wt/AzK</sub> was performed on a MicroCa VP-ITC 353  
Isothermal Titration Calorimeter (ITC; MicroCalITC200, 354  
Malvern Panalytical, Malvern, UK) as described in ref 47. 355  
For flow cytometry analysis, HT-29 or LS-174 cells were 356  
detached from the culture dish with 2 mL of 0.05% trypsin- 357  
EDTA (1x) solution for 10 min at 37 °C. Afterward, cells were 358  
counted and transferred to a U-bottom 96-well plate (Sarstedt 359  
AG & Co. KG, Numbrecht, North Rhine-Westphalia, 360  
Germany) to a concentration of 1 × 10<sup>5</sup> cells/well. To 361  
compare the binding of STxB<sub>wt</sub> AF647 and mutant STxB<sub>AzK</sub> 362  
AF647 to cell surface receptors, cells were incubated with 363  
lectins for 30 min on ice, while PBS-treated cells were set as 364  
the negative control. Subsequently, cells were centrifuged at 365  
1600g for 3 min on ice and washed twice with fluorescence- 366  
activated cell sorting (FACS) buffer (PBS supplemented with 367  
3% FBS v/v). When unlabeled STxB<sub>wt</sub>, STxB<sub>AzK</sub>, or STxB<sub>AzK</sub>- 368  
DBCO-PEG4-Val-Cit-PAB-MMAE was used, cells were 369  
stained with a fluorescently labeled anti-6-His epitope tag 370  
Alexa Fluor 647 antibody diluted in FACS buffer to monitor 371  
the presence of the lectins at the surface. Incubation was 372  
carried out for 20 min on ice and protected from light. At the 373  
end of incubation, cells were centrifuged and washed twice as 374  
described above. After the last washing step, the cells were 375  
resuspended in FACS buffer and transferred to FACS tubes 376  
(Kisker Biotech GmbH Co. KG, Steinfurt, North Rhine- 377  
Westphalia, Germany). The fluorescence intensity of treated 378  
cells was monitored immediately at FACS Gallios (Beckman 379  
Coulter Inc., Indianapolis, USA) and further analyzed using 380  
FlowJo V.10.5.3 (FlowJo LLC, BD). 381

**Immunofluorescence and Epifluorescence Imaging.** 382  
Between 5 and 6 × 10<sup>4</sup> HT-29 cells were seeded on 12 mm 383  
glass coverslips in a 4-well plate and allowed to adhere. The 384  
next day, cells were stimulated with fluorescently labeled 385  
STxB<sub>wt</sub> AF647 or STxB<sub>AzK</sub> AF647 (0.13 μM) for 30 min at 4 386  
°C and then washed once with PBS and incubated at 37 °C for 387  
the indicated times. Subsequently, cells were fixed with ice-cold 388  
methanol for 8 min at –20 °C. Cells were blocked with 3% 389  
(w/v) BSA in PBS for 30 min and incubated with target 390  
primary antibodies (1:100) for 1 h at RT. After three washes, 391  
cells were stained with fluorescently labeled secondary 392  
antibodies (1:200) for 30 min at RT in the dark. Nuclei 393  
were counterstained with DAPI (5 × 10<sup>–9</sup> g/L), and the 394  
samples were mounted on coverslips using Mowiol (containing 395  
the antibleaching reagent DABCO). Samples were imaged 396  
using a Nikon ECLIPSE Ti2 inverted microscope, a 60× oil 397  
immersion objective, and a numerical aperture (NA) of 1.40. 398

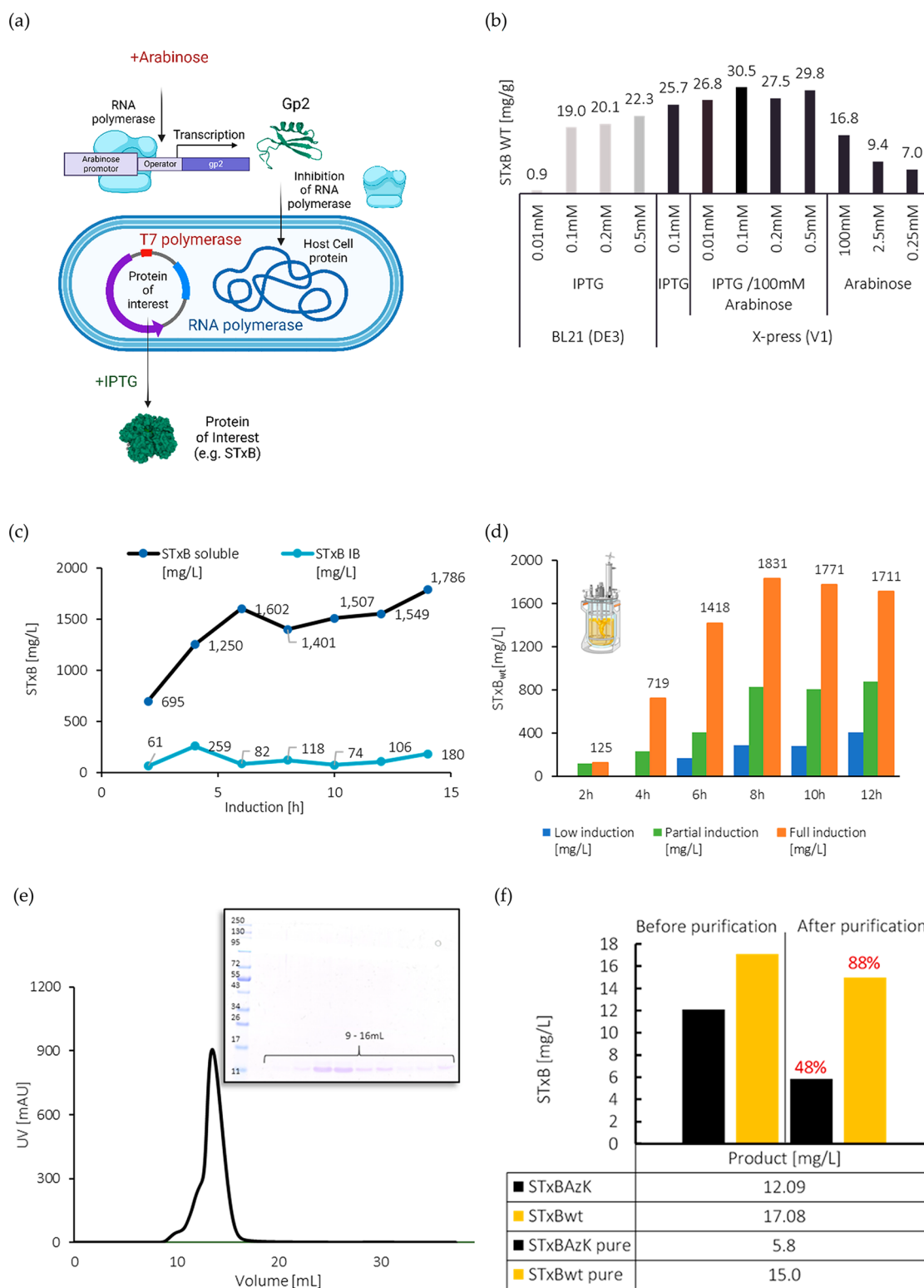


**Figure 2.** Manufacturing process established with STxB<sub>wT</sub>. (a) enGenes-X-press technology that allows for controlled decoupling of recombinant protein production. (b) Specific yields (mg STxB/g CDM) of STxB<sub>wT</sub> (pET30a-Cer) production in  $\mu$ -bioreactor cultivations of the BL21 (DE3) and V1 strains induced at different IPTG (0.01–0.5 mM) and Ara (0.25–100 mM) concentrations. (c) Course of STxB<sub>wT</sub> (pET30a-Cer) production; volumetric yields (mg/L) of soluble and inclusion body fraction from a 1 L benchtop scale-fed batch process of the V1 strain and pulse induction (0.5 mM IPTG and 100 mM Ara). (d) Volumetric yield (mg/L) of soluble STxB<sub>wT</sub> (pET30a-Cer) produced in benchtop cultures with V1 with a combination of pulse and feed induction (Ara 100 mM + IPTG low (0.01 mM) or partial (0.1 mM) or full (0.5 mM)). (e) Purification of STxB<sub>wT</sub> with SEC chromatography (pentamer) and corresponding SDS-PAGE (STxB monomer of 11 kDa). (f) Final yields before versus after purification of STxB<sub>AzK</sub> (pSCS-T7  $\times$  31) produced using a condition optimized by pET30a<STxB<sub>wT</sub>>Cer plasmid in comparison to pSCS-T7  $\times$  31<STxB<sub>wT</sub>>. The percentage (red) indicates the product remaining after purification. Graphical representation created with BioRender.com.

399 The images were further analyzed using ImageJ 1.53 from  
400 Laboratory for Optical and Computational Instrumentation. A  
401 minimum of  $\geq 20$  cells per condition were analyzed.

402 **Luciferase-Based Cytotoxicity Assay.** For the bio-  
403 luminescence-based cytotoxicity assay, luciferase-expressing  
404 HT-29 and LS-174 tumor cells were counted and plated at a  
405 concentration of  $1 \times 10^4$  cells in 96-well white flat bottom  
406 plates in triplicates. The next day, 75  $\mu\text{g}/\text{mL}$  of D-firefly  
407 luciferin potassium salt was diluted in a complete medium and  
408 added to the tumor cells. Bioluminescence (BLI) was  
409 measured in the luminometer (Tecan infinity M200 Pro) to  
410 establish the BLI baseline. Subsequently, the treatment was  
411 added at several concentrations (DBCO-PEG4-Val-Cit-PAB-  
412 MMAE: 1 nM, 5 nM, 10 nM; STxB<sub>AzK</sub>: 1.3 nM, 6.5 nM, 26  
413 nM, 52 nM; STxB<sub>AzK</sub>-DBCO-PEG4-Val-Cit-PAB-MMAE: 1.3  
414 nM, 6.5 nM, 26 nM, 52 nM) to the samples, as indicated, and  
415 BLI was recorded at several times (24, 48, or 72 h) after  
416 incubation at 37 °C. BLI was measured as relative light units  
417 (RLUs). RLU signals from tumor cells cultured in the absence  
418 of any treatment determine spontaneous cell death. RLU  
419 signals from cells treated with 2% Triton X-100 indicate  
420 maximal cell death. The percent of specific killings was  
421 calculated using the following formula:

$$\% \text{ of specific killing} = 100 \times \left( \frac{\text{RLU}_{\text{average spontaneous death}} - \text{RLU}_{\text{test}}}{\text{RLU}_{\text{average spontaneous death}} - \text{RLU}_{\text{average maximal death}}} \right)$$

422 **Cell Proliferation (MTT) Assay.** To determine IC<sub>50</sub> values  
423 for STxB<sub>AzK</sub>-MMAE, HT-29 or LS-174 cells were treated with  
424 increasing concentrations of the STxB<sub>AzK</sub>-drug conjugate for  
425 72 h in a standard MTT assay. An amount of  $3 \times 10^4$  cells per  
426 well was transferred to a 96-well plate with a U-bottom. The  
427 cells were centrifuged at 1600g for 3 min at RT. The cell pellet  
428 was then resuspended in 100  $\mu\text{L}$  of variously concentrated  
429 STxB<sub>AzK</sub>-MMAE solutions (1.3, 2.6, 6.5, 13, 19.5, 26, 39, 52,  
430 and 65 nM) and transferred to a 96-well flat-bottomed plate.  
431 The cells were incubated for 72 h at 37 °C. Subsequently, 10  
432  $\mu\text{L}$  of MTT-labeling solution (MTT Cell Proliferation Kit,  
433 Roche) was added to each well, and the cells were incubated  
434 for 4 h at 37 °C. Then, 100  $\mu\text{L}$  of the solubilization reagent was  
435 added to each well, and the plate was incubated at 37 °C  
436 overnight. The next day, the absorbance of the samples was  
437 measured at 550 nm using a BioTek microplate reader. The  
438 data were further analyzed using GraphPad 6.01 Prism  
439 software.

440 **Statistical Analysis.** All data in the graphs are presented as  
441 mean  $\pm$  standard deviation (SD) and were calculated from the  
442 results of biological experiments. Statistical testing was  
443 performed with GraphPad Prism 6.01 software and Microsoft  
444 Excel 365 using data of  $\geq 3$  biological replicates. Statistical  
445 differences in independent, identical samples were determined  
446 with a two-tailed, unpaired *t* test. Tests with a *p*-value  $\leq 0.05$   
447 are considered statistically significant and marked with an  
448 asterisk (\*). Nonsignificant results are indicated with ns.

## 449 ■ RESULTS AND DISCUSSION

450 **STxB Production and Optimization.** To elucidate  
451 suitable production conditions for anticipated low-expressing  
452 STxB<sub>AzK</sub>, we began the optimization of STxB<sub>wt</sub> production  
453 using a standard expression vector (pET30a-Cer). Our  
454 objectives were to implement production process improve-  
455 ments that yield high STxB production before introducing  
456 orthogonal pairs (pSCS-T7  $\times$  31 vector) for introducing the

AzK inside the STxB amino acid sequence, with production 457  
imposing extensive demands on the overall production process 458  
of this STxB<sub>AzK</sub> carrier. 459

The process development was performed in five steps 460  
comprising: (1) optimizing STxB<sub>wt</sub> production in V1 versus 461  
BL21 (DE3) at the  $\mu$ -scale; (2) upscaling the best performing 462  
strain to a 1 L benchtop scale; (3) optimizing the induction 463  
condition at the benchtop scale; (4) setting up the purification 464  
strategy and stability test for storage; and (5) transferring the 465  
manufacturing condition from the STxB<sub>wt</sub> to STxB<sub>AzK</sub> variant 466  
expressed from the pSCS-T7  $\times$  31 plasmid (Supporting 467  
Information Figure 1b). 468

The V1 strain provided higher quantities of soluble STxB 469  
(Figure 2b) and therefore was selected for further production 470  
optimization. The addition of arabinose (Ara) upon induction 471  
led to transcription and then the translation of a phage-derived 472  
protein, called Gp2.<sup>48</sup> This protein is a phage-derived inhibitor 473  
of *E. coli* RNA polymerase that stops the V1 strain from further 474  
generating biomass. The growth decouples, and the addition of 475  
IPTG drives the production of the protein of interest. This 476  
resulted in differences in STxB production between wt BL21 477  
(DE3) (22.3 mg/g CDM) which has lower expression 478  
capabilities than the V1 strain (29.8 mg/g CDM) at induction 479  
with 0.5 mM IPTG (Supporting Information Figure 2a). This 480  
corresponded to 189.8 mg/L and 256.4 mg/L, respectively. 481  
However, the highest production by V1 was at 0.1 mM IPTG 482  
(30.5 mg/g CDM; 269.1 mg/L), where the productivity 483  
reaches a plateau (0.1–0.5 mM). Cultures, where V1 was 484  
supplemented with Ara only (100–0.25 mM), showed lower 485  
expression of STxB<sub>wt</sub> in comparison to other induction 486  
conditions with IPTG supplementation. The V1 strain induced 487  
at 0.5 mM IPTG and 100 mM Ara was identified as the best- 488  
performing system in  $\mu$ -scale and subsequently used in all 489  
bench-scale cultivations. Additionally, we show the accumu- 490  
lation of STxB<sub>wt</sub> in soluble and insoluble (IBs) forms over the 491  
course of the cultivation (Figure 2c), which was calculated 492  
using SDS-PAGE gels under reducing conditions (Supporting 493  
Information Figure 2b). It was a pulse induction directly into 494  
the production reactor resulting in a 1786 mg/L final yield of 495  
soluble STxB<sub>wt</sub>. We estimated that changing the delivery of 496  
inducer from pulse to a combination of pulse and feed 497  
induction could improve the STxB<sub>wt</sub> productivity, and 498  
therefore we tested low (0.01 mM), partial (0.1 mM), and 499  
full induction (0.5 mM) IPTG concentrations introduced 500  
steadily by combining feed and pulse induction (Figure 2d). 501  
With this approach, we supplemented a steady influx of 502  
inducers after the induction time point. This method has 503  
proven resourceful for reaching maximal production at 8 h 504  
(1831 mg/L). 505

At the end of fermentation, the harvested, centrifuged, and 506  
purified cells (homogenizer and IMAC) were separated with 507  
an analytical SEC column. We have observed a characteristic 508  
elution peak at 45 kDa (pentamer) that corresponds to the 509  
single band (monomer under reducing condition) on SDS- 510  
PAGE. This is likely due to polydispersity or hydrodynamic 511  
contributions of the STxB molecule, as the asymmetric shape 512  
of the peak was only observed with the STxB pentamer when 513  
compared to other proteins.<sup>49</sup> As some STxB tends to 514  
aggregate, the purity of nonaggregated pentamer was measured 515  
and detected at 92% using MALS-SEC (−80 °C storage, 516  
Supporting Information Figure 3a). After 2 weeks of storage at 517  
4 °C, the STxB<sub>wt</sub> started to degrade to 85% purity (Supporting 518  
Information Figure 3b); however, a small filtration step could 519

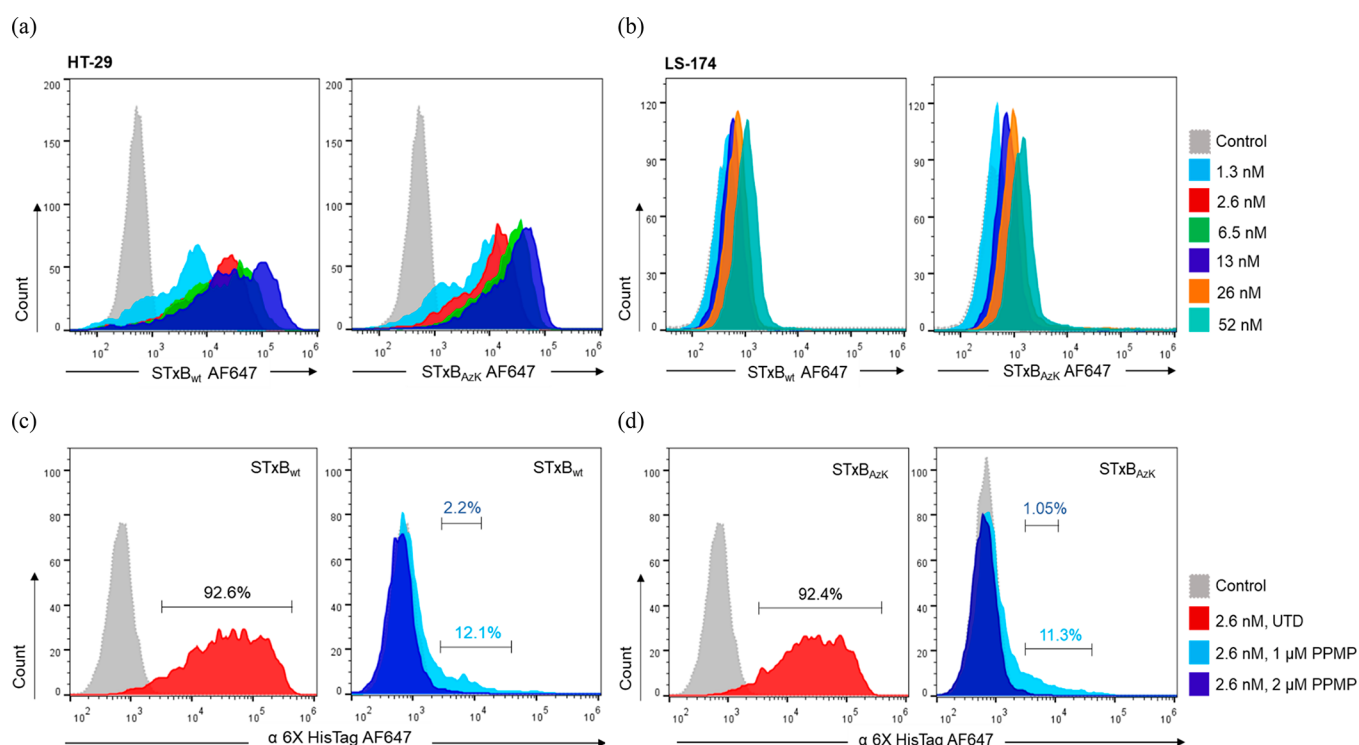


**Figure 3.** Binding of STxB<sub>wt</sub> and STxB<sub>AzK</sub> to HT-29 and LS-174 colon cancer cells. (a) Representative histograms of flow cytometry analysis of gated living HT-29 cells stained with increasing concentrations of fluorescently labeled STxB<sub>wt</sub> AF647 (left) or STxB<sub>AzK</sub> AF647 (right) for 30 min on ice. (b) Histograms of fluorescence intensity of gated living LS-174 cells incubated with increasing concentrations of STxB<sub>wt</sub> AF647 (left) or STxB<sub>AzK</sub> AF647 (right) for 30 min on ice. (c) Histograms of fluorescence intensity of Gb3<sup>+</sup> HT-29 cells incubated with 2.6 nM STxB<sub>wt</sub> in the absence (UTD, left plot) or presence (right panel) of the GLS synthesis inhibitor PPMP. Cells were incubated with STxB<sub>wt</sub> for 30 min on ice and stained with anti-6-His epitope tag AF647 antibody for 20 min on ice to assess the presence of STxB<sub>wt</sub> at the surface. At 72 h post-treatment with 1 and 2  $\mu$ M PPMP, STxB<sub>wt</sub> no longer binds to HT-29 cells, confirming the depletion of Gb3 from the surface. (d) Histograms of fluorescence intensity of Gb3<sup>+</sup> HT-29 cells incubated with 2.6 nM STxB<sub>AzK</sub> followed by staining with the anti-6-His epitope tag AF647 antibody as described above. Histograms on the left panel show binding of STxB<sub>AzK</sub> to Gb3 exposed at the surface (UTD) after 30 min incubation on ice. On the right plot, flow cytometry analysis of HT-29 cells pretreated with PPMP for 72 h and incubated with STxB<sub>AzK</sub> (as indicated before) is illustrated. In the absence of Gb3, the binding of the protein to the plasma membrane is drastically reduced, confirming its specificity toward the Gb3 antigen. The number of cells within the live population (y-axis) is plotted against the fluorescence intensity of the (a, b) STxB<sub>wt/AzK</sub> AF647 or (c, d) anti-6-His epitope tag AF647. Percentages in (c, d) indicate the number of cells positive for the tested STxB<sub>wt/AzK</sub>.

520 remove unwanted storage-brought impurities (Supporting  
521 Information Figure 3c). Furthermore, storage at  $-20^{\circ}\text{C}$  and  
522  $-80^{\circ}\text{C}$  prevented detectable degradation (data not shown),  
523 and repeated defrosting (4-times) from  $-20^{\circ}\text{C}$  storage led to  
524 no significant change in purity (Supporting Information Figure  
525 3d). Samples were stored at  $-20^{\circ}\text{C}$ , and storage experiments  
526 were supplemented with isothermal titration calorimetry  
527 (ITC) prior to carrying out additional experiments (Support-  
528 ing Information Figure 4). These methods became our quality  
529 measurements for testing the biological activity of STxB  
530 protein directly after manufacturing and before conducting *in*  
531 *vitro* analysis. This included (1) V1 strain cultivation to 37 g/L  
532 CDM and production for 8 h with induction by feed and pulse  
533 (0.5 mM IPTG and 100 mM Ara); (2) homogenization,  
534 centrifugation, filtration, IMAC, and SEC purification; and (3)  
535 storage at  $-20^{\circ}\text{C}$ . The only difference in STxB<sub>AzK</sub> production  
536 was the addition of 5 mM AzK to the feed. The production of  
537 STxB<sub>AzK</sub> produced in pSCS-T7  $\times$  31 was significantly lower  
538 (Figure 2f) than STxB<sub>wt</sub> produced in pET30a-Cer and will  
539 require further optimization. Our observation shows that upon  
540 purification there is a loss of up to 48% of the final product.  
541 This is expected, as the plasmid contains not only the STxB  
542 sequence but also the orthogonal pair. The production of  
543 coexpressed proteins is more demanding than the single

544 expression carried out by standard pET30a-Cer. We wish to  
545 solve this problem by integrating the orthogonal pair in the  
546 genome under different strength promoters and ribosome  
547 binding sites. With this approach, we will be able to express  
548 STxB<sub>AzK</sub> with the pET30a-Cer vector.

**Evaluation of STxB<sub>AzK</sub> Receptor Recognition and Specificity on Human Colon Cancer Cell Lines HT-29 and LS-174.** To monitor the potential of STxB<sub>AzK</sub> as a carrier  
551 for targeted drug delivery, we evaluated its functionality in  
552 binding to human colon adenocarcinoma cells. HT-29 and LS-  
553 174 are well-characterized cell lines with epithelial morphology  
554 and are widely used as preclinical model systems. Moreover,  
555 recent studies from Meléndez et al.<sup>42</sup> have described the  
556 abundance and species diversity of the Gb3 antigen of HT-29  
557 and LS-174 cells, among other model cancer cell lines. As a  
558 result, the amount of Gb3 isoforms was found to be very high  
559 in HT-29 cells, while LS-174 displayed low traces of the  
560 antigen. In order to confirm the Gb3 abundance at the plasma  
561 membrane of these cells, fluorescently labeled STxB-Cy5 from  
562 commercial sources was used in flow cytometry assays, further  
563 providing a benchmark control (Supporting Information  
564 Figure 5).

To assess the capacity of STxB<sub>AzK</sub> to target the  
566 glycosphingolipid Gb3 specifically, we compared its binding  
567

568 activity to the STxB<sub>wt</sub> generated in this study. HT-29 and LS-  
569 174 cells were screened in flow cytometry analysis to detect the  
570 binding of STxB variants (Figure 3). STxB<sub>wt</sub> was randomly  
571 labeled with AlexaFluor 647 NHS ester in a standard reaction.  
572 The STxB<sub>AzK</sub> was conjugated to a DBCO-containing Alexa  
573 Fluor 647 probe via SPAAC reaction. Following protein  
574 purification, the degree of labeling was estimated spectropho-  
575 tometrically, and it resulted in the attachment of ~2.8 and  
576 ~2.1 fluorescent dyes to the STxB<sub>wt</sub> and STxB<sub>AzK</sub> pentamers,  
577 respectively. HT-29 cells were then stained with four  
578 increasing concentrations of STxB<sub>wt</sub> AF647 or STxB<sub>AzK</sub>  
579 AF647 (1.3, 2.6, 6.5, 13 nM) for 30 min on ice. Then, the  
580 unbound STxB was washed away to decrease nonspecific  
581 signals, and samples were analyzed via flow cytometry (Figure  
582 3a). The flow cytometry analysis revealed a strong binding of  
583 STxB<sub>wt</sub> (left plot) and STxB<sub>AzK</sub> (right plot) to Gb3<sup>+</sup> HT-29  
584 cells, starting from concentrations in the low nanomolar range.  
585 This is visible in a clear shift of the histograms of fluorescence  
586 intensity toward higher values. The STxB<sub>wt</sub> and STxB<sub>AzK</sub>  
587 showed a highly similar, dose-dependent binding pattern to  
588 the plasma membrane of cells, suggesting the retained affinity  
589 of the STxB mutant toward the Gb3 antigen.

590 Next, we characterized the binding of STxB<sub>wt/AzK</sub> to LS-174  
591 cells, which exhibit a low density of the Gb3 antigen at the  
592 surface. Figure 3b shows a flow cytometry analysis of LS-174  
593 cells stained with STxB<sub>wt</sub> AF647 (left plot) or STxB<sub>AzK</sub> AF647  
594 (right plot). The graphs illustrate the absence of binding by  
595 STxB<sub>wt/AzK</sub> to the plasma membrane for concentrations lower  
596 than 10 nM. When higher concentrations of STxB<sub>wt/AzK</sub> were  
597 applied (13–52 nM), a shift of the histograms toward higher  
598 values of fluorescence intensity was registered, suggesting a  
599 basal presence of Gb3 at the cell surface. The identical binding  
600 patterns registered for both protein variants on these two cell  
601 lines further support the identity of STxB<sub>wt</sub> and STxB<sub>AzK</sub>  
602 produced in this study.

603 To further assess the specificity of STxB<sub>AzK</sub> toward the  
604 tumor-related Gb3 antigen, Gb3<sup>+</sup> HT-29 cells were treated  
605 with the glucosylceramide synthase (GCS) inhibitor PPMP.<sup>46</sup>  
606 PPMP resembles the structure of endogenous ceramide and its  
607 product GlcCer and acts as an effective inhibitor of GCS. To  
608 this end, GCS is considered a pivotal metabolic target enzyme  
609 to clear away ceramides.<sup>50</sup> As a result, PPMP helps sustain a  
610 high level of ceramide inside cells by inhibiting its conversion  
611 to glucosylated ceramide. To effectively inhibit the synthesis of  
612 glucosylceramide-based GSLs and thus deplete Gb3, HT-29  
613 were treated with 1 or 2 μM PPMP for 72 h<sup>44</sup> before flow  
614 cytometry analysis. Subsequently, cells were incubated with 2.6  
615 nM STxB<sub>wt</sub> to confirm the depletion of Gb3 from the plasma  
616 membrane. On the left plot of Figure 3c, the typical histogram  
617 of binding of STxB<sub>wt</sub> is visible for untreated cells (UTD). At 72  
618 h post-treatment with 1 μM PPMP, the same concentration of  
619 STxB<sub>wt</sub> (2.6 nM, right plot) did not elicit a notable shift of the  
620 histogram toward higher fluorescence intensities, thus  
621 revealing a highly reduced binding of STxB<sub>wt</sub> to the surface  
622 of cells. More interestingly, at a concentration of 2 μM PPMP,  
623 STxB<sub>wt</sub> was no longer detected at the membrane of treated  
624 cells. STxB<sub>wt</sub> binding to cancer cells was decreased by more  
625 than 90% compared to the untreated control, suggesting a  
626 successful depletion of the Gb3 antigen from the plasma  
627 membrane. Similarly, the binding of STxB<sub>AzK</sub> illustrated in  
628 Figure 3d, resembles the one observed for STxB<sub>wt</sub>. In the  
629 absence of Gb3 at the surface, the AzK variant was no longer  
630 able to recognize HT-29 cells (right plot), confirming the

exquisite specificity of the generated STxB<sub>AzK</sub> toward the 631  
tumor-associated Gb3 antigen. 632

These observations are in line with the studies conducted by 633  
Rosato et al.<sup>44</sup> The two STxB variants—wild-type and AzK— 634  
were compared for their binding specificity and affinity on a 635  
panel of Burkitt's lymphoma-derived cells and colon 636  
adenocarcinoma cell lines, confirming the specificity of the 637  
STxB mutant upon AzK incorporation. The STxB<sub>AzK</sub> was 638  
found to be highly selective for Gb3<sup>+</sup> tumor cell lines and 639  
successfully targeted them for elimination, while sparing Gb3<sup>-</sup> 640  
or Gb3-depleted cells. 641

### STxB<sub>AzK</sub>-Mediated Delivery of MMAE to Colon- 642 Derived Cancer Cells and *in Vitro* Tumor Elimination. 643

Given the aberrant expression of several GSLs in cancer, 644  
glycan-binding proteins represent a powerful tool for the 645  
development of novel targeting strategies. As a proof-of- 646  
concept, we have investigated the ability of the generated 647  
STxB<sub>AzK</sub> to deliver the antineoplastic agent MMAE to colon- 648  
cancer-derived cell lines by targeting the tumor-related Gb3 649  
antigen. In such a context, STxB represents an optimal carrier 650  
with a nanomolar affinity for its receptor, which renders it a 651  
suitable vehicle for efficient delivery to target cells. Indeed, the 652  
homopentameric STxB can interact with up to 15 Gb3 653  
molecules, with high avidity ( $K_d = 10^9 \text{ M}^{-1}$ ).<sup>8,25</sup> 654

The DBCO-PEG4-Val-Cit-PAB-MMAE (Supporting Infor- 655  
mation Figure 6) was conjugated to STxB<sub>AzK</sub> in three different 656  
molar ratios (1:5, 1:10, and 1:20) in a standardized SPAAC 657  
reaction. The successful attachment of the prodrug to STxB<sub>AzK</sub> 658  
pentamers was confirmed with MS (Supporting Information 659  
Figure 7). We evaluated the intracellular accumulation of 660  
STxB<sub>AzK</sub> in HT-29 cells via immunofluorescence studies 661  
(Supporting Information Figure 8) and confirmed the ability 662  
of the protein to induce its uptake in target cells. Here, the 663  
intracellular distribution of STxB<sub>wt/AzK</sub> was monitored at 3 h 664  
after incubation, and lysosomes were stained with antibodies 665  
directed against LAMP1 to assess the presence of the STxB in 666  
the target compartment. Fluorescence imaging revealed that 667  
the STxB<sub>AzK</sub> variant, similarly to its wild-type counterpart, can 668  
be found in the intracellular space of Gb3<sup>+</sup> target cells at 3 h 669  
postincubation. We registered a limited extent of signal overlap 670  
between the carrier and the lysosomes of target cells, 671  
highlighted by the arrows in Supporting Information Figure 672  
8b. However, a clear colocalization between STxB<sub>AzK</sub> and the 673  
degradative compartment of HT-29 could not be confirmed. 674  
The trafficking route of the STxB<sub>wt/AzK</sub> within this cell line 675  
remains elusive and requires further investigation in the future. 676  
Nevertheless, we hypothesized that STxB<sub>AzK</sub> following its 677  
uptake could mediate the specific delivery of DBCO-PEG4- 678  
Val-Cit-PAB-MMAE to the intracellular environment of colon- 679  
derived cancer cells, ultimately resulting in tumor cell 680  
elimination. We cultured Gb3<sup>+</sup> HT-29 cells in the presence 681  
of DBCO-PEG4-Val-Cit-PAB-MMAE, STxB<sub>AzK</sub> or the con- 682  
jugated STxB<sub>AzK</sub>-DBCO-PEG4-Val-Cit-PAB-MMAE (1:10)— 683  
referred to as STxB<sub>AzK</sub>-MMAE from now on—for 72 h, and 684  
elimination of target cells was recorded as bioluminescence 685  
(BLI) at several time points (24, 48, and 72 h). BLI- 686  
cytotoxicity assays offer a robust and fast evaluation of the cell 687  
viability of luciferase-transduced cell lines, in the presence of 688  
specific cytotoxic treatments. For this purpose, HT-29 and LS- 689  
174 cells were stably transduced to express luciferase.<sup>44</sup> Since 690  
BLI is ATP-dependent, dying cells stop emitting BLI once its 691  
remaining intracellular ATP has been used up. Thus, cellular 692  
cytotoxicity can be detected as a decrease in BLI.<sup>51,52</sup> Here, 693

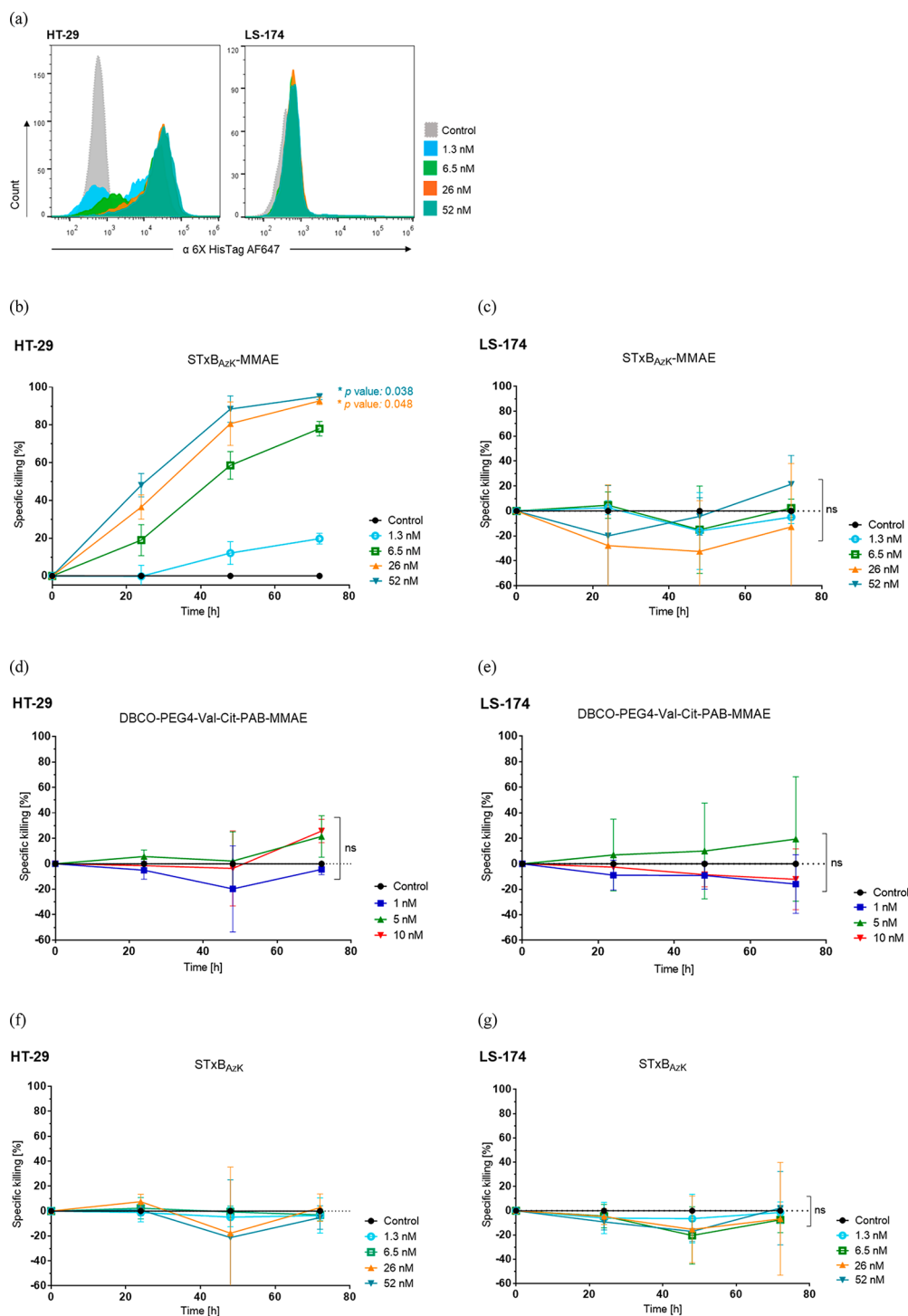
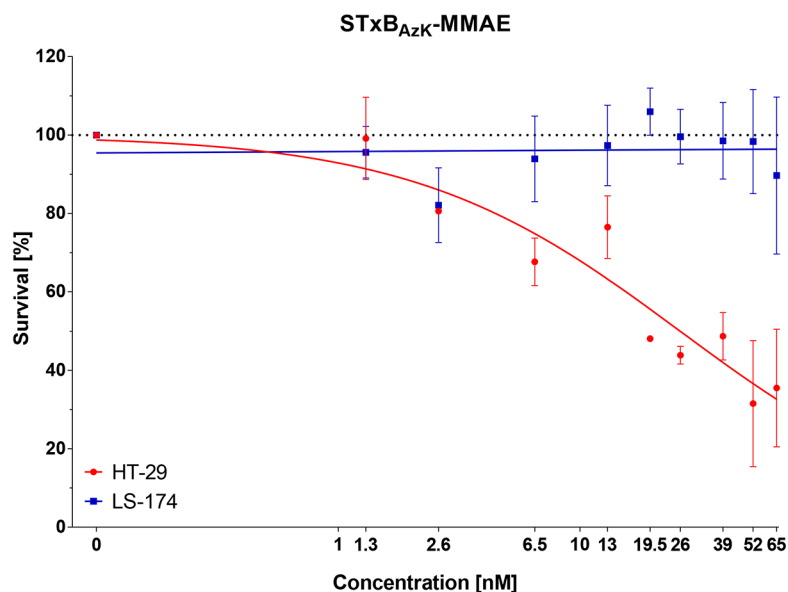


**Figure 4.** STxB<sub>AzK</sub>-mediated drug delivery to HT-29 and LS-174 tumor cells and *in vitro* specific killing. Tumour cell recognition and quantification of specific killing for HT-29 and LS-174 target cells incubated with STxB<sub>AzK</sub> after conjugation to MMAE. (a) Representative histograms of flow cytometry analysis of gated living HT-29 cells (left plot) or LS-174 cells (right plot) incubated with increasing concentrations of STxB<sub>AzK</sub> after attachment of DBCO-PEG4-Val-Cit-PAB-MMAE in a SPAAC reaction (molar ratio 1:10). Cells were incubated with the STxB<sub>AzK</sub>-MMAE conjugate for 30 min on ice, followed by secondary labeling with the anti-6-His epitope tag AF647 antibody for 20 min on ice to detect the presence of STxB<sub>AzK</sub> at the plasma membrane. The number of cells within the live population (*y*-axis) is plotted against the fluorescence intensity of the anti-6-His epitope tag AF647 (*x*-axis). (b) Cytotoxicity assay of HT-29 cells or (c) LS-174 cells cultured with 1.3, 6.5, 26, or 52 nM STxB<sub>AzK</sub>-MMAE for 72 h. (d) Cytotoxicity assay of HT-29 cells or (e) LS-174 cells cultured with 1, 5, or 10 nM free DBCO-PEG4-Val-Cit-PAB-MMAE for 72 h. (f) Cytotoxicity assay of HT-29 cells or (g) LS-174 cells incubated with unconjugated STxB<sub>AzK</sub> for 72 h. The percentage of viability was calculated relative to the luminescence from an equal number of input control cells and used to calculate the percentage of specific killing. Results are expressed as a mean  $\pm$  SD ( $n = 3$ ) from 3 separate experiments. Statistical differences in independent samples were determined with a two-tailed, unpaired *t* test for control and treatment groups, at each time point. Tests with a *p*-value  $\leq 0.05$  are considered statistically significant and marked with an asterisk (\*). Nonsignificant results are indicated as ns.

(a)



(b)

Cell line	Compound	IC <sub>50</sub> [nM]
HT-29 (Gb3 <sup>+</sup> )	StxB <sub>AzK</sub> -MMAE	25.89
LS-174 (Gb3 <sup>-</sup> )	StxB <sub>AzK</sub> -MMAE	/

**Figure 5.** Cytotoxic activity of STxB<sub>AzK</sub>-MMAE on Gb3<sup>+</sup> HT-29 and Gb3<sup>-</sup> LS-174 tumor cells. (a) Dose-dependent reduction of HT-29 (red) and LS-174 (blue) cell survival following the addition of STxB<sub>AzK</sub>-MMAE in a standard cell proliferation assay (MTT) for 72 h compared to treatment with PBS. Data represent three independent experiments,  $n = 3$ . (b) IC<sub>50</sub> values for STxB<sub>AzK</sub>-MMAE efficacy following dose–response cytotoxicity curves presented in (a).

694 control samples included target cells incubated in the absence  
 695 of any treatment, counted as spontaneous cell death. Figure 4  
 696 presents graphs of *in vitro* killing activity, expressed as a  
 697 percentage of specific killing induced by the three treatments.  
 698 Upon conjugation of STxB<sub>AzK</sub> to DBCO-PEG4-Val-Cit-PAB-  
 699 MMAE, we first ensured that the attachment of the drug to  
 700 STxB<sub>AzK</sub> did not interfere with its binding functionality and  
 701 receptor recognition. Flow cytometry analysis of STxB<sub>AzK</sub>-  
 702 MMAE (1:10) revealed a consistent shift in fluorescence  
 703 intensity upon treatment of cells with the STxB<sub>AzK</sub>-drug  
 704 conjugate (Figure 4a, left plot). The recognition of Gb3  
 705 antigen at the plasma membrane followed a similar pattern to  
 706 the one reported in Figure 3a, with a dose-dependent binding  
 707 of STxB<sub>AzK</sub> to the cell surface. Strikingly, Gb3<sup>+</sup> HT-29 cells  
 708 were efficiently eliminated by the treatment starting from low  
 709 nanomolar concentrations (Figure 4b). In the presence of the  
 710 6.5 nM STxB<sub>AzK</sub>-MMAE conjugate, we recorded ~50% of  
 711 specific tumor cells killing at 48 h post-treatment, culminating  
 712 in 72% of effective tumor cell elimination at 72 h. The higher  
 713 concentrations (26 and 52 nM) induced cell death at earlier  
 714 time points, starting from 24 h (approximately 50% cell death)  
 715 and resulting in nearly complete tumor cell elimination—up to  
 716 94%—at 72 h. The STxB<sub>AzK</sub>-MMAE conjugates (1:5) and  
 717 (1:20) were also investigated for their ability to induce specific  
 718 killing of HT-29 cells over 72 h of treatment. The activity of

the two conjugates in mediating tumor cell death was  
 comparable to the one reported for STxB<sub>AzK</sub>-MMAE (1:10),  
 as illustrated in Supporting Information Figure 9.

To confirm that the observed tumor cell killing was  
 mediated exclusively by the STxB<sub>AzK</sub>-drug conjugates, we  
 further investigated tumor cell cytotoxicity in the presence of 1,  
 5, or 10 nM free DBCO-PEG4-Val-Cit-PAB-MMAE (Figure  
 4d). Treatment with the prodrug in the absence of a carrier did  
 not induce the effective killing of tumor cells. At 72 h, we  
 recorded mild cytotoxicity when cells were incubated with 5  
 nM or 10 nM DBCO-PEG4-Val-Cit-PAB-MMAE, reaching an  
 average of 20% tumor cell death. Similarly, treatment with the  
 STxB<sub>AzK</sub> carrier alone (1.3, 6.5, 26, or 52 nM) did not induce  
 cell death (Figure 4f). The cells retained viability and exhibited  
 proliferation when coincubated with STxB<sub>AzK</sub> for 72 h, further  
 confirming the safety of this carrier for biomedical develop-  
 ment. Similar studies of STxB-induced cytotoxic activity were  
 also reported by Batisse et al.,<sup>41</sup> who synthesized a series of  
 STxB-MMA conjugates and observed receptor-dependent  
 elimination of Gb3<sup>+</sup> HT-29 cells, as opposed to free MMA  
 compounds. The main difference between this conjugation  
 from our approach was that the attachment of a drug requires  
 more steps at harsher chemical reaction conditions. The  
 STxB<sub>AzK</sub>-mediated *in vitro* targeting of tumor cells presented  
 here is significantly relevant and suggests efficient delivery of

744 the toxic payload to the intracellular environment, along with  
745 its correct release.

746 Moreover, we monitored the specific killing activity of the  
747 STxB<sub>AzK</sub>-MMAE conjugate in the presence of a low density of  
748 Gb3 antigen on the surface of LS-174 cells. According to the  
749 observations previously described (Figure 3b), LS-174 exhibits  
750 only a trace amount of this GSL, providing additional control  
751 for the specificity of the STxB<sub>AzK</sub> carrier. Upon attachment of  
752 the prodrug to STxB<sub>AzK</sub>, analysis performed in flow cytometry  
753 with the STxB<sub>AzK</sub>-MMAE conjugate did not reveal off-target  
754 interaction with LS-174 cells nor loss of protein functionality  
755 (Figure 4a, right plot). Nevertheless, the binding pattern of  
756 STxB<sub>AzK</sub>-MMAE was highly similar to the one described earlier  
757 in Figure 3b. For protein concentrations <10 nM, the STxB<sub>AzK</sub>-  
758 MMAE conjugate could be detected at the surface of LS-174  
759 cells, as illustrated in the histograms of fluorescence intensity in  
760 Figure 4a. At each concentration, a slight but consistent  
761 increase in binding to LS-174 cells was registered. The minimal  
762 binding of STxB<sub>AzK</sub>-MMAE is reflected in the graph of specific  
763 STxB<sub>AzK</sub>-mediated killing reported in Figure 4c. In the same  
764 experimental setup, LS-174 cells were incubated with STxB<sub>AzK</sub>-  
765 MMAE (1:10) for 72 h, and elimination of target cells was  
766 recorded at 24, 48, and 72 h. Control samples included target  
767 cells incubated in the absence of treatment and determined  
768 spontaneous cell death. In contrast to what we observed for  
769 HT-29, LS-174 cells did not show substantial cytotoxicity upon  
770 treatment with STxB<sub>AzK</sub>-MMAE. Cells retained their viability,  
771 and for doses <10 nM, proliferation was observed. Indeed, cell  
772 growth for treated samples was comparable to the negative  
773 control and is indicated by the negative values on the Y-axis. At  
774 the highest dose (52 nM), around 20% of cell cytotoxicity was  
775 recorded, accounting for a basal expression of the Gb3 antigen  
776 at the plasma membrane. Accordingly, similar observations  
777 were collected in cytotoxicity assays of LS-174 cells incubated  
778 with the STxB<sub>AzK</sub>-MMAE conjugate (1:5) and (1:20), shown  
779 in Supporting Information Figure 10. On the other hand,  
780 samples treated with DBCO-PEG4-Val-Cit-PAB-MMAE (1, 5,  
781 or 10 nM, Figure 4e) or a STxB<sub>AzK</sub> carrier (1.3, 6.5, 26, or 52  
782 nM, Figure 4g) did not display consistent cytotoxicity over the  
783 72 h of incubation, further confirming the results reported for  
784 HT-29 cells.

785 The luciferase-killing assay was complemented by a second  
786 *in vitro* cytotoxicity assay designed to estimate the half-maximal  
787 inhibitory concentration (IC<sub>50</sub>) of the STxB<sub>AzK</sub>-MMAE  
788 conjugate. To this end, a standard colorimetric assay based  
789 on the metabolic activity of treated cells was used. The assay  
790 relies on the cleavage of tetrazolium salt MTT to form a  
791 formazan dye by live cells displaying enzymatic activity,  
792 suitable for quantifying cell proliferation and viability. Upon  
793 treatment with increasing concentrations of STxB<sub>AzK</sub>-MMAE  
794 (1:10) (Figure 5a) for 72 h, the absorbance of treated samples  
795 was measured with a spectrophotometer to determine cell  
796 viability. The STxB<sub>AzK</sub>-MMAE conjugate (1.3–65 nM)  
797 displayed significant cytotoxicity on Gb3<sup>+</sup> HT-29 cells, further  
798 confirming the results described in Figure 4b. Importantly,  
799 Gb3<sup>-</sup> LS-174 cells preserved their viability upon incubation  
800 with the STxB<sub>AzK</sub>-drug conjugate, indicating once more the  
801 specificity of STxB<sub>AzK</sub> toward the tumor-associated antigen  
802 Gb3. According to these results, we determined the IC<sub>50</sub> for  
803 the STxB<sub>AzK</sub>-drug conjugate to define the drug's efficacy. The  
804 IC<sub>50</sub> is a most widely used informative measure of the amount  
805 of drug needed to inhibit by half a biological process,  
806 represented in this case by tumor cell survival (Figure 5c).

The IC<sub>50</sub> value for STxB<sub>AzK</sub>-MMAE on HT-29 falls in the low  
nanomolar range (25.89 nM). These results document the  
efficiency of the Gb3-specific targeting and intracellular  
delivery using STxB<sub>AzK</sub> as carrier for the toxic payload.

The data confirm that the receptor-mediated drug delivery  
system generated in this study enables specific MMAE delivery  
to Gb3-expressing tumor cells and correct intracellular drug  
release, while maintaining the drug's cytotoxic activity. On the  
contrary, the killing activity of the free prodrug DBCO-PEG4-  
Val-Cit-PAB-MMAE reported in Figure 4d,e was Gb3-  
independent. The treatment failed to distinguish between  
target and nontarget cells. LS-174 cells, expressing poor or no  
Gb3 at the surface, were equally eliminated by the standard  
MMAE treatment, while their viability was preserved following  
incubation with STxB<sub>AzK</sub>-MMAE.

## CONCLUSIONS

In this work, we have established a platform for the production  
and *in vitro* analysis of a drug delivery system for Gb3<sup>+</sup> colon  
cancer cells. The STxB<sub>AzK</sub> mutant was expressed with the  
pSCS-T7 × 31 plasmid, produced in a 1 L benchtop reactor in  
fed-batch mode, purified with two-step purification steps and  
conjugated to the MMAE-containing prodrug DBCO-PEG4-  
Val-Cit-PAB-MMAE, a precursor of ADCs. The manufacturing  
of STxB<sub>wt</sub> (in pET30a-Cer plasmid) was first produced at the  
highest yield reaching 1786 mg/L after 12 h. The production  
was improved by changing the conventional pulse induction  
strategy (0.5 mM pulsed into the reactor) and combining it  
with induction to the feeding system (0.5 mM divided between  
feed and reactor). The maximal yield of STxB<sub>wt</sub> was not only  
increased to 1831 mg/L but as well achieved 4 h earlier (8 h).  
This strategy applied to the manufacturing of STxB<sub>AzK</sub> (pSCS-  
T7 × 31 plasmid) resulted in much lower yields of 12.09 mg/L  
due to a more demanding expression platform (coexpression of  
orthogonal pair). The presence of a unique reactive handle—  
namely AzK—in STxB<sub>AzK</sub> enabled the attachment of the pro-  
drug at predefined positions in the STxB pentamer, thereby  
avoiding interference with its carbohydrate-binding sites. The  
STxB<sub>wt/AzK</sub> variants exhibit high specificity for the Gb3 antigen  
when compared to Gb3<sup>-</sup> cells, where no or poor binding was  
observed. The binding analysis performed with flow cytometry  
was augmented with a luciferase-based killing assay to quantify  
the ability of STxB<sub>AzK</sub> to deliver the antitumoral drug  
intracellularly. The drug delivery system, STxB<sub>AzK</sub>-DBCO-  
PEG4-Val-Cit-PAB-MMAE (1:10), successfully crossed the  
plasma membrane to release the MMAE drug intracellularly  
and mediated tumor cell death at 72 h with an efficiency as  
high as 94% and an estimated IC<sub>50</sub> of 25.89 nM.

Overall, these observations further support the specificity of  
the generated carrier toward the tumor-related Gb3 antigen  
and strengthen the hypothesis that STxB<sub>AzK</sub> is highly efficient  
in mediating a targeted delivery of antitumoral drugs to cancer  
cells. Relatively simple click chemistry reactions enable the  
carrier presented in this study to be conjugated to a toxic  
payload in a highly selective, site-specific, and efficient manner.  
Moreover, the toxic moiety in the STxB<sub>AzK</sub>-drug conjugate  
can be readily exchanged with the purpose of delivering drugs  
characterized by diverse mechanisms of action. The attach-  
ment of drugs to STxB<sub>AzK</sub> is indeed not limited to small  
molecules but can be extended to silencing RNAs, peptides, or  
even antibody fragments. The versatility of this tool is  
combined to a well-defined control over the drug attachment,  
as the sites for STxB modification are designed strategically to

869 be far away from the glycan-binding site, preserving the lectin's  
870 specificity toward the antigen of interest.

871 It is important to mention that the glycosphingolipid Gb3 is  
872 also commonly indicated as the Burkitt's lymphoma-associated  
873 antigen (BLA), as it is highly expressed on Burkitt's lymphoma  
874 (BL) cells.<sup>53</sup> This opens the window for an extended and more  
875 comprehensive investigation of the STxB-mediated drug  
876 delivery presented here. It would be essentially interesting to  
877 evaluate the efficacy of an antitumor treatment based on the  
878 STxB<sub>AzK</sub> carrier targeting the Gb3 antigen on a panel of  
879 different human tumor types, including both hematological  
880 and solid tumors. This proof-of-concept study could provide  
881 significant benefits to the treatment of additional solid tumors,  
882 as they have been mostly difficult to target with clinical success.  
883 Gb3 overexpression in breast,<sup>54,55</sup> ovarian,<sup>56</sup> and pancre-  
884 atic<sup>57,58</sup> carcinomas can provide the basis for further  
885 application of this tool in the future. Nonetheless, it is of  
886 crucial importance to consider that Gb3 is present on the  
887 plasma membrane of several nontransformed cells, potentially  
888 leading to off-target cytotoxicity upon treatment with STxB<sub>AzK</sub>-  
889 MMAE. Moreover, the difference in Gb3 isoforms and  
890 abundance among healthy or transformed cells plays a key  
891 role in the STxB receptor recognition and could affect the  
892 outcome of the therapy.<sup>42,51,59-61</sup> STxB binding and specific  
893 intracellular transport within Gb3<sup>+</sup> cells are highly influenced  
894 by the heterogeneity of Gb3 in terms of chain length, degree of  
895 saturation, and hydroxylation of its fatty acyl chain, along with  
896 its distribution within lipid rafts of the plasma membrane.<sup>34,62</sup>  
897 This structural variability would suggest a screening of target  
898 cells to determine the Gb3 heterogeneity before considering  
899 such a therapeutic choice.

900 Further studies to address the stability of STxB<sub>AzK</sub>  
901 conjugates in plasma need to be conducted, to estimate the  
902 half-life of the compounds and their sensitivity to catabolism.  
903 Moreover, the exact intracellular trafficking route exploited by  
904 the carrier in target cells needs to be elucidated to gain a  
905 further understanding of the molecular mechanism of action of  
906 the STxB<sub>AzK</sub>-drug conjugate. Additionally, while the *in vitro*  
907 studies display encouraging properties of the STxB<sub>AzK</sub>-drug  
908 model system, *in vivo* mouse tumor models are required to gain  
909 further insight into the specific tumor elimination mediated by  
910 the STxB<sub>AzK</sub> carrier.<sup>63,64</sup> The *in vivo* half-life and pharmaco-  
911 kinetic properties of the STxB<sub>AzK</sub>-MMAE conjugate will likely  
912 determine if this approach can be successfully employed as a  
913 therapeutic. The molecular weight of the conjugate (~45 kDa)  
914 is below the renal excretion threshold, constituting a risk of  
915 enhancing its clearance rate, thereby decreasing its therapeutic  
916 effect. Nonetheless, the fast kinetics of STxB uptake into target  
917 cells has the potential to counteract renal excretion if the  
918 treatment is designed for a site-specific application to reach the  
919 solid tumor. Additionally, while in the past decades researchers  
920 have exploited numerous carbohydrate-binding toxins as drug  
921 delivery systems, these carriers are at high risk of eliciting an  
922 immune response as a side effect. The clinical success of  
923 recombinant immunotoxins (RITs) in patients with a normal  
924 immune system is indeed limited by their immunogenicity.<sup>65</sup>  
925 Extensive studies of STx functions have highlighted its  
926 interaction with antigen presenting cells (APCs), predom-  
927 inantly dendritic cells and macrophages, resulting in APC  
928 stimulation and major histocompatibility complex (MHC)  
929 classes I and II expression.<sup>66</sup> This is accompanied by the  
930 induction of inflammatory cytokine secretion, such as IL-1, IL-  
931 6, and TNF- $\alpha$ , by macrophages.<sup>67</sup> The STxB carrier combined

to an API might drive the activation of the immune system and  
the production of neutralizing antibodies (NAbs) by  
interacting with the Gb3 antigens expressed on APCs and B  
cells, hampering repeated cycles of treatment and constituting  
a high risk for the patient. However, STxB-induced activation  
of dendritic cells results in enhanced CD8<sup>+</sup> T cell functionality,  
which can aid tumor surveillance.<sup>68</sup> The need for balancing the  
immunogenicity of STxB in tumor therapy becomes evident  
with the activation of immune cells that can further enhance  
the antitumor efficacy. Draft Guidance for Industry Assay  
Development for Immunogenicity Testing of Therapeutic  
Proteins has recently been published by the US FDA and  
provide detailed guidelines for a comprehensive evaluation of  
immunogenicity that should be monitored systematically and  
on a case-by-case basis.<sup>69</sup> In this case, immunogenicity of the  
STxB carrier may arise from the presence of nonhuman  
sequences or epitopes contained in the polypeptide. Moreover,  
the absence of glycosylation or an altered pattern of  
glycosylation can expose cryptic B-cell and T-cell epitopes in  
the protein that cause the protein to appear foreign to the  
immune system.<sup>70</sup> *In silico* and *in vitro* techniques allow  
putative B-cell and T-cell epitopes to be identified and  
eliminated in candidate molecules while maintaining structure  
and function. An alternative would be to prevent helper T-cell  
activation by interfering with MHC II presentation or T-cell  
recognition. As an example, other strategies have also been  
developed to control the immunogenicity of therapeutic  
monoclonal antibodies (mAbs) based on increasing the  
human sequence content and include framework human-  
ization, chimerization, and use of mice with humanized  
germlines to decrease the rate of NAbs in mice.<sup>71</sup> Other  
approaches to mitigate the immunogenicity of therapeutic  
proteins include PEGylation to mask the immunogenic  
epitopes or combination therapy with immune suppressive  
molecules that can be toxic and limit the treatment. Each of  
these strategies could be applied in an attempt to decrease  
STxB<sub>AzK</sub> immunogenicity *in vivo*. As a highly critical risk factor,  
neutralization of cancer treatments by the immune system  
should be taken into account in the development of STxB-  
drug conjugates in future steps.

Additionally, as other lectins of different origins have been  
identified for their selective recognition of the Gb3 antigen,<sup>62</sup>  
further development in the field of lectin-mediated targeted  
drug delivery is imaginable. For example, the lectin LecA from  
*Pseudomonas aeruginosa*<sup>72</sup> or the engineered lectin Mitsuba  
from *Mytilus galloprovincialis*<sup>34,64</sup> has been already described to  
successfully target Gb3<sup>+</sup> tumor cell lines<sup>42</sup> and offer  
opportunities for clinical advancement.

In conclusion, these studies showed that the ready-to-click  
STxB<sub>AzK</sub> carrier offers the possibility to target glycan epitopes  
on tumor cells and deliver drugs effective in current cancer  
therapies, providing an effective appliance for targeted drug  
delivery in cancer research.

## ■ ASSOCIATED CONTENT

### Data Availability Statement

The data sets generated and/or analyzed during the current  
study are available from the corresponding authors upon  
reasonable request.

### Supporting Information

Supplementary 1: Design of (a) pET30a < STxB<sub>wt</sub> > Cer, (b)  
pSCS-T7  $\times$  3 < STxB<sub>wt</sub> > or pSCS-T7  $\times$  3 < STxB<sub>AzK</sub> >.  
Supplementary 2: SDS-PAGE gel of STxB<sub>wt</sub> expression

994 optimization. Supplementary 3: SEC-MALS stability measure-  
 995 ment of STxB<sub>wt</sub>. Supplementary 4. ITC measurement of  
 996 STxB<sub>wt/AzK</sub> binding to Gb3 receptor. Supplementary 5.  
 997 Expression of Gb3 antigens at the surface of HT-29 and LS-  
 998 174 tumor cells. Supplementary 6. Intact protein MS analysis  
 999 of STxB<sub>AzK</sub> (8959 Da) and DBCO-PEG4-Cit-PAB-MMAE  
 1000 drug attachment (10615 Da). Supplementary 7. Composition  
 1001 of DBCO-PEG4-Val-Cit-PAB-MMAE toxic payload delivered  
 1002 to Gb3-expressing cancer cells by STxB<sub>AzK</sub>. Supplementary 8.  
 1003 Fluorescence imaging of HT-29 cells incubated with  
 1004 STxB<sub>wt/AzK</sub>. Supplementary 9. STxB<sub>AzK</sub>-MMAE conjugates  
 1005 (1:5) and (1:20) mediate cytotoxic drug delivery to HT-29  
 1006 tumor cells and the in vitro-specific killing. Supplementary 9.  
 1007 STxB<sub>AzK</sub>-MMAE conjugates (1:5) and (1:20) mediate cytotoxic  
 1008 drug delivery to HT-29 tumor cells and the in vitro-specific  
 1009 killing. Supplementary 10. STxB<sub>AzK</sub>-MMAE conjugates (1:5) and  
 1010 (1:20) mediate cytotoxic drug delivery to LS-174 tumor cells  
 1011 and in vitro killing. The Supporting Information is available  
 1012 free of charge at [https://pubs.acs.org/doi/10.1021/acsome-](https://pubs.acs.org/doi/10.1021/acsomega.3c00667)  
 1013 [ga.3c00667](https://pubs.acs.org/doi/10.1021/acsomega.3c00667).

(PDF)

## 1015 ■ AUTHOR INFORMATION

### 1016 Corresponding Author

1017 **Juergen Mairhofer** – *enGenes Biotech GmbH, 1190 Vienna,*  
 1018 *Austria*; [orcid.org/0000-0002-2686-1971](https://orcid.org/0000-0002-2686-1971);  
 1019 Email: [juergen.mairhofer@engenes.com](mailto:juergen.mairhofer@engenes.com)

### 1020 Authors

1021 **Natalia Danielewicz** – *enGenes Biotech GmbH, 1190 Vienna,*  
 1022 *Austria; Department of Biotechnology, University of Natural*  
 1023 *Resources and Life Sciences, 1190 Vienna, Austria*

1024 **Francesca Rosato** – *Faculty of Biology, University of Freiburg,*  
 1025 *79104 Freiburg, Germany; Signaling Research Centers*  
 1026 *BIOSS and CIBSS, University of Freiburg, 79104 Freiburg,*  
 1027 *Germany*

1028 **Jana Tomisch** – *Faculty of Biology, University of Freiburg,*  
 1029 *79104 Freiburg, Germany; Signaling Research Centers*  
 1030 *BIOSS and CIBSS, University of Freiburg, 79104 Freiburg,*  
 1031 *Germany*

1032 **Jonas Gräber** – *Faculty of Biology, University of Freiburg,*  
 1033 *79104 Freiburg, Germany; Signaling Research Centers*  
 1034 *BIOSS and CIBSS, University of Freiburg, 79104 Freiburg,*  
 1035 *Germany*

1036 **Birgit Wiltschi** – *Department of Biotechnology, University of*  
 1037 *Natural Resources and Life Sciences, 1190 Vienna, Austria;*  
 1038 *Austrian Centre of Industrial Biotechnology (ACIB), 1190*  
 1039 *Vienna, Austria*; [orcid.org/0000-0001-5230-0951](https://orcid.org/0000-0001-5230-0951)

1040 **Gerald Striedner** – *Department of Biotechnology, University*  
 1041 *of Natural Resources and Life Sciences, 1190 Vienna, Austria*

1042 **Winfried Römer** – *Faculty of Biology, University of Freiburg,*  
 1043 *79104 Freiburg, Germany; Signaling Research Centers*  
 1044 *BIOSS and CIBSS, University of Freiburg, 79104 Freiburg,*  
 1045 *Germany; Freiburg Institute for Advanced Studies (FRIAS),*  
 1046 *University of Freiburg, 79104 Freiburg, Germany*

1047 Complete contact information is available at:

1048 <https://pubs.acs.org/doi/10.1021/acsomega.3c00667>

### 1049 Author Contributions

1050 Conceptualization of the study, N.D., F.R., W.R., and J.M.;  
 1051 methodology, N.D., F.R., J.T., J.G., G.S., W.R., B.W., and J.M.;  
 1052 formal analysis, N.D., F.R., J.T., and J.G.; investigation, N.D.

and F.R.; data curation, N.D., F.R., J.T., and J.G.; writing—  
 original draft preparation, N.D. and F.R.; writing—review and  
 editing, N.D., F.R., B.W., G.S., W.R., and J.M.; supervision,  
 W.R. and J.M.; project administration, J.M.; funding  
 acquisition, J.M. and W.R. All authors have read and agreed  
 to the published version of the manuscript.

### 1059 Author Contributions

1060 <sup>†</sup>These authors contributed equally.

### 1061 Funding

1062 This research was funded by the European Union's Horizon  
 1063 2020 Research and Innovation Program, under the Marie  
 1064 Skłodowska–Curie grant agreement synBIOcarb (No.  
 1065 814029). Moreover, W.R. acknowledges support by the  
 1066 Deutsche Forschungsgemeinschaft (DFG, German Research  
 1067 Foundation) under Germany's Excellence Strategy (EXC-  
 1068 2189) and from the Major Research Instrumentation (project  
 1069 number: 438033605) by the Ministry for Science, Research  
 1070 and Arts of the State of Baden-Württemberg (Az: 33-7532.20)  
 1071 and by the Freiburg Institute for Advanced Studies (FRIAS).

### 1072 Notes

1073 LRS chambers used as blood sources were purchased from the  
 1074 blood bank of the University Medical Centre Freiburg  
 1075 (approval of the University Freiburg Ethics Committee: 147/  
 1076 15).

1077 The authors declare the following competing financial  
 1078 interest(s): Juergen Mairhofer is CEO and CSO of enGenes  
 1079 Biotech, a company providing technology, IP, and fee-for-  
 1080 service in the field of recombinant protein expression.

## 1081 ■ ACKNOWLEDGMENTS

1082 We thank PD Dr. Susana Minguet from the University of  
 1083 Freiburg, Germany, for providing the luciferase-expressing HT-  
 1084 29 and LS-174 cells used in this study. We also express  
 1085 gratitude to Dr. Pavel Salavei of the CIBSS Signaling Factory,  
 1086 University of Freiburg, Germany, for his help and guidance in  
 1087 flow cytometry. We further thank Rajeev Pasupuleti from the  
 1088 Austrian Centre of Industrial Biotechnology, Graz, Austria, for  
 1089 providing pSCS\_T7 × 31 plasmid.

## 1090 ■ ABBREVIATIONS

ADCs	Antibody–drug conjugates	1091
API	Active pharmaceutical ingredient	1092
AzK	Azido lysine	1093
BLA	Burkitt's lymphoma-associated antigen	1094
BLI	Bioluminescence	1095
DBCO	Dibenzocyclooctyne	1096
DMEM	Dulbecco's modified eagle medium	1097
FACS	Fluorescence-activated cell sorting	1098
FDA	Food and Drug Administration	1099
Gb3	Globotriaosylceramide	1100
GCS	Glucosylceramide synthase	1101
GSL	Glycosphingolipid	1102
IC <sub>50</sub>	Half-maximal inhibitory concentration	1103
mAbs	Monoclonal antibodies	1104
MMAE	Monomethyl auristatin E	1105
NAbs	Neutralizing antibodies	1106
ncAA	Noncanonical amino acid	1107
PBS	Phosphate-buffered saline	1108
PEG	Polyethylene glycol	1109
PPMP	1-Phenyl-2-palmitoylamino-3-morpholino-1- propanol	1110
RLU	Relative light units	1111

1112	RTIs	Recombinant immunotoxins
1113	SDS-PAGE	Sodium dodecyl sulfate-polyacrylamide gel electrophoresis
1114	SPAAC	Strain-promoted azide-alkyne cycloaddition
1115	STxB	Shiga toxin B subunit
1116	STxB <sub>AzK</sub>	Shiga toxin B subunit azido lysine
1118	STxB <sub>wt</sub>	Shiga toxin B subunit wild-type

## 1119 ■ REFERENCES

1120 (1) Tiwari, G.; Tiwari, R.; Bannerjee, S.; Bhati, L.; Pandey, S.;  
 1121 Pandey, P.; Sriwastawa, B. Drug Delivery Systems: An Updated  
 1122 Review. *Int. J. Pharm. Investig.* **2012**, *2* (1), 2.  
 1123 (2) Vargason, A. M.; Anselmo, A. C.; Mitragotri, S. The Evolution of  
 1124 Commercial Drug Delivery Technologies. *Nat. Biomed. Eng.* **2021**, *5*  
 1125 (9), 951–967.  
 1126 (3) Liu, G.; Yang, L.; Chen, G.; Xu, F.; Yang, F.; Yu, H.; Li, L.;  
 1127 Dong, X.; Han, J.; Cao, C.; Qi, J.; Su, J.; Xu, X.; Li, X.; Li, B. A Review  
 1128 on Drug Delivery System for Tumor Therapy. *Front. Pharmacol.* **2021**,  
 1129 *12*, 1–22.  
 1130 (4) Majumdar, S.; Siahaan, T. J. Peptide-Mediated Targeted Drug  
 1131 Delivery. *Med. Res. Rev.* **2012**, *32*, 637–658.  
 1132 (5) Flygare, J. A.; Pillow, T. H.; Aristoff, P. Antibody-Drug  
 1133 Conjugates for the Treatment of Cancer. *Chem. Biol. Drug Des.*  
 1134 **2013**, *81*, 113–121.  
 1135 (6) Khongorzul, P.; Ling, C. J.; Khan, F. U.; Ihsan, A. U.; Zhang, J.  
 1136 Antibody - Drug Conjugates : A Comprehensive Review. *Mol. Cancer*  
 1137 *Res.* **2020**, *18* (18), 3–19.  
 1138 (7) Lambert, J. M.; Chari, R. V. J. Ado-Trastuzumab Emtansine (T-  
 1139 DM1): An Antibody - Drug Conjugate (ADC) for HER2-Positive  
 1140 Breast Cancer. *Am. Chem. Soc.* **2014**, *57*, 6949–6964.  
 1141 (8) Drago, J. Z.; Modi, S.; Chandralapaty, S. Unlocking the Potential  
 1142 of Antibody-Drug Conjugates for Cancer Therapy. *Nat. Rev. Clin.*  
 1143 *Oncol.* **2021**, *18*, 327–344.  
 1144 (9) Luginbuehl, V.; Meier, N.; Kovar, K.; Rohrer, J. Intracellular  
 1145 Drug Delivery: Potential Usefulness of Engineered Shiga Toxin  
 1146 Subunit B for Targeted Cancer Therapy. *Biotechnol. Adv.* **2018**, *36*  
 1147 (3), 613–623.  
 1148 (10) Robert, A.; Wiels, J. Shiga Toxins as Antitumor Tools. *Toxins*  
 1149 *(Basel)*. **2021**, *13* (10), 690.  
 1150 (11) Danielewicz, N.; Rosato, F.; Dai, W.; Römer, W.; Turnbull, W.  
 1151 B.; Mairhofer, J. *Microbial Carbohydrate-Binding Toxins - From*  
 1152 *Etiology to Biotechnological Application*. **2022**, *59* (April), 107951.  
 1153 (12) Johannes, L.; Römer, W. Shiga Toxins from Cell Biology to  
 1154 Biomedical Applications. *Nat. Rev. Microbiol.* **2010**, *8* (2), 105–116.  
 1155 (13) Römer, W.; Berland, L.; Chambon, V.; Gaus, K.; Windschiegel,  
 1156 B.; Tenza, D.; Aly, M. R. E.; Fraissier, V.; Florent, J. C.; Perrais, D.;  
 1157 Lamaze, C.; Raposo, G.; Steinem, C.; Sens, P.; Bassereau, P.;  
 1158 Johannes, L. Shiga Toxin Induces Tubular Membrane Invaginations  
 1159 for Its Uptake into Cells. *Nature* **2007**, *450* (7170), 670–675.  
 1160 (14) Windschiegel, B.; Orth, A.; Romer, W.; Berland, L.; Stechmann,  
 1161 B.; Bassereau, P.; Johannes, L.; Steinem, C. Lipid Reorganization  
 1162 Induced by Shiga Toxin Clustering on Planar Membranes. *PLoS One*  
 1163 **2009**, *4* (7), 1–11.  
 1164 (15) Mallard, F.; Antony, C.; Tenza, D.; Salamero, J.; Goud, B.;  
 1165 Johannes, L. Direct Pathway from Early/Recycling Endosomes to the  
 1166 Golgi Apparatus Revealed through the Study of Shiga Toxin B-  
 1167 Fragment Transport. *J. Cell Biol.* **1998**, *143* (4), 973–990.  
 1168 (16) Sandvig, K.; Kavaliuskiene, S.; Skotland, T. The Protein  
 1169 Toxins Ricin and Shiga Toxin as Tools to Explore Cellular  
 1170 Mechanisms of Internalization and Intracellular Transport. *Toxins*  
 1171 *(Basel)*. **2021**, *13* (6), 377.  
 1172 (17) Liu, Y.; Tian, S.; Thaker, H.; Dong, M. Shiga Toxins: An  
 1173 Update on Host Factors and Biomedical Applications. *Toxins (Basel)*.  
 1174 **2021**, *13* (3), 222.  
 1175 (18) Liu, Z.; Li, X.; Lu, Z.; Qin, X.; Hong, H.; Zhou, Z.; Pieters, R.  
 1176 J.; Shi, J.; Wu, Z. *Repurposing the Pentameric B-Subunit of Shiga Toxin*  
 1177 *for Gb3-Targeted Immunotherapy of Colorectal Cancer by Rhamnose*  
 1178 *Conjugation*. **2022**, *111* (10), 2719–2729.

(19) Kostova, V.; Dransart, E.; Azoulay, M.; Brulle, L.; Bai, S. K.;  
 Florent, J. C.; Johannes, L.; Schmidt, F. Targeted Shiga Toxin-Drug  
 Conjugates Prepared via Cu-Free Click Chemistry. *Bioorg. Med. Chem.*  
**2015**, *23* (22), 7150–7157.  
 (20) Casas, M. G.; Stargardt, P.; Mairhofer, J.; Wiltschi, B.  
 Decoupling Protein Production from Cell Growth Enhances the  
 Site-Specific Incorporation of Noncanonical Amino Acids in  
 E. Coli. *ACS Synth. Biol.* **2020**, *9* (11), 3052–3066.  
 (21) Danielewicz, N.; Dai, W.; Rosato, F.; Webb, M. E.; Striedner,  
 G.; Römer, W.; Turnbull, W. B.; Mairhofer, J. In-Depth Character-  
 ization of a Re-Engineered Cholera Toxin Manufacturing Process  
 Using Growth-Decoupled Production in Escherichia Coli. *Toxins*  
*(Basel)*. **2022**, *14* (6), 396.  
 (22) Dorywalska, M.; Strop, P.; Melton-Witt, J. A.; Hasa-Moreno,  
 A.; Farias, S. E.; Galindo Casas, M.; Delaria, K.; Lui, V.; Poulsen, K.;  
 Loo, C.; Krimm, S.; Bolton, G.; Moine, L.; Dushin, R.; Tran, T. T.;  
 Liu, S. H.; Rickert, M.; Foletti, D.; Shelton, D. L.; Pons, J.; Rajpal, A.  
 Effect of Attachment Site on Stability of Cleavable Antibody Drug  
 Conjugates. *Bioconjugate Chem.* **2015**, *26* (4), 650–659.  
 (23) Yoneda, Y.; Steiniger, S. C. J.; Capková, K.; Mee, J. M.; Liu, Y.;  
 Kaufmann, G. F.; Janda, K. D. A Cell-Penetrating Peptidic GRP78  
 Ligand for Tumor Cell-Specific Prodrug Therapy. *Bioorg. Med. Chem.*  
*Letts.* **2008**, *18* (5), 1632–1636.  
 (24) Dubowchik, G. M.; Firestone, R. A.; Padilla, L.; Willner, D.;  
 Hofstead, S. J.; Mosure, K.; Knipe, J. O.; Lasch, S. J.; Trail, P. A.  
 Cathepsin B-Labile Dipeptide Linkers for Lysosomal Release of  
 Doxorubicin from Internalizing Immunoconjugates: Model Studies of  
 Enzymatic Drug Release and Antigen-Specific in Vitro Anticancer  
 Activity. *Bioconjugate Chem.* **2002**, *13* (4), 855–869.  
 (25) Lee, M.-S.; Koo, S.; Jeong, D.; Tesh, V. Shiga Toxins as Multi-  
 Functional Proteins: Induction of Host Cellular Stress Responses,  
 Role in Pathogenesis and Therapeutic Applications. *Toxin* **2016**, *8*  
 (3), 77.  
 (26) Zhao, R. Y.; Wilhelm, S. D.; Audette, C.; Jones, G.; Leece, B.  
 A.; Lazar, A. C.; Goldmacher, V. S.; Singh, R.; Kovtun, Y.; Widdison,  
 W. C.; Lambert, J. M.; Chari, R. V. J. Synthesis and Evaluation of  
 Hydrophilic Linkers for Antibody-Maytansinoid Conjugates. *J. Med.*  
*Chem.* **2011**, *54* (10), 3606–3623.  
 (27) Pabst, M.; McDowell, W.; Manin, A.; Kyle, A.; Camper, N.; De  
 Juan, E.; Parekh, V.; Rudge, F.; Makwana, H.; Kantner, T.; Parekh,  
 H.; Michelet, A.; Sheng, X. B.; Popa, G.; Tucker, C.; Khayrabad, F.;  
 Pollard, D.; Kozakowska, K.; Resende, R.; Jenkins, A.; Simoes, F.;  
 Morris, D.; Williams, P.; Badescu, G.; Baker, M. P.; Bird, M.; Frigerio,  
 M.; Godwin, A. Modulation of Drug-Linker Design to Enhance in  
 Vivo Potency of Homogeneous Antibody-Drug Conjugates. *J.*  
*Controlled Release* **2017**, *253*, 160–164.  
 (28) Wang, Y.; Liu, L.; Fan, S.; Xiao, D.; Xie, F.; Li, W.; Zhong, W.;  
 Zhou, X. Antibody-Drug Conjugate Using Ionized CYS-Linker-Mmae  
 as the Potent Payload Shows Optimal Therapeutic Safety. *Cancers*  
*(Basel)*. **2020**, *12* (3), 744.  
 (29) Bryant, P.; Pabst, M.; Badescu, G.; Bird, M.; McDowell, W.;  
 Jamieson, E.; Swierkosz, J.; Jurlewicz, K.; Tommasi, R.; Henseleit, K.;  
 Sheng, X.; Camper, N.; Manin, A.; Kozakowska, K.; Peciak, K.;  
 Laurine, E.; Grygorash, R.; Kyle, A.; Morris, D.; Parekh, V.; Abhilash,  
 A.; Choi, J. W.; Edwards, J.; Frigerio, M.; Baker, M. P.; Godwin, A. In  
 Vitro and in Vivo Evaluation of Cysteine Rebridged Trastuzumab-  
 MMAE Antibody Drug Conjugates with Defined Drug-to-Antibody  
 Ratios. *Mol. Pharmaceutics* **2015**, *12* (6), 1872–1879.  
 (30) Dornan, D.; Bennett, F.; Chen, Y.; Dennis, M.; Eaton, D.;  
 Elkins, K.; French, D.; Go, M. A. T.; Jack, A.; Junutula, J. R.;  
 Koepfen, H.; Lau, J.; McBride, J.; Rawstron, A.; Shi, X.; Yu, N.; Yu, S.  
 F.; Yue, P.; Zheng, B.; Ebens, A.; Polson, A. G. Therapeutic Potential  
 of an Anti-CD79b Antibody-Drug Conjugate, Anti-CD79b-vc-  
 MMAE, for the Treatment of Non-Hodgkin Lymphoma. *Blood*  
**2009**, *114* (13), 2721–2729.  
 (31) Koga, Y.; Manabe, S.; Aihara, Y.; Sato, R.; Tsumura, R.; Iwafuji,  
 H.; Furuya, F.; Fuchigami, H.; Fujiwara, Y.; Hisada, Y.; Yamamoto, Y.;  
 Yasunaga, M.; Matsumura, Y. Antitumor Effect of Antitissue Factor

- 1247 Antibody-MMAE Conjugate in Human Pancreatic Tumor Xenografts. *Int. J. Cancer* **2015**, *137* (6), 1457–1466.
- 1248 (32) Mohseni, Z.; Sedighian, H.; Halabian, R.; Amani, J.; Behzadi, E.; Imani Fooladi, A. A. Potent in Vitro Antitumor Activity of B-Subunit of Shiga Toxin Conjugated to the Diphtheria Toxin against Breast Cancer. *Eur. J. Pharmacol.* **2021**, 899 (March), 174057.
- 1253 (33) Simons, K.; Ikonen, E. Functional Rafts in Cell Membranes. *Nature* **1997**, *387* (6633), 569–572.
- 1255 (34) Falguières, T.; Mallard, F.; Baron, C.; Hanau, D.; Lingwood, C.; Goud, B.; Salameró, J.; Johannes, L. Targeting of Shiga Toxin B-Subunit to Retrograde Transport Route in Association with Detergent-Resistant Membranes. *Mol. Biol. Cell* **2001**, *12* (8), 2453–2468.
- 1260 (35) Schüller, S. Shiga Toxin Interaction with Human Intestinal Epithelium. *Toxins (Basel)*. **2011**, *3* (6), 626–639.
- 1262 (36) El Alaoui, A.; Schmidt, F.; Amessou, M.; Sarr, M.; Decaudin, D.; Florent, J. C.; Johannes, L. Shiga Toxin-Mediated Retrograde Delivery of a Topoisomerase I Inhibitor Prodrug. *Angew. Chemie - Int. Ed.* **2007**, *46* (34), 6469–6472.
- 1266 (37) Mellor, G. E.; Goulter, R. M.; Chia, T. W. R.; Dykes, G. A. Comparative Analysis of Attachment of Shiga-Toxicogenic Escherichia Coli and Salmonella Strains to Cultured HT-29 and Caco-2 Cell Lines. *Appl. Environ. Microbiol.* **2009**, *75* (6), 1796–1799.
- 1270 (38) Kirn, T. J.; Jude, B. A.; Taylor, R. K. A Colonization Factor Links Vibrio Cholerae Environmental Survival and Human Infection. *Nature* **2005**, *438* (7069), 863–866.
- 1273 (39) Pinho, S. S.; Reis, C. A. Glycosylation in Cancer: Mechanisms and Clinical Implications. *Nat. Rev. Cancer* **2015**, *15* (9), 540–555.
- 1275 (40) Celi, A. B.; Goldstein, J.; Rosato-Siri, M. V.; Pinto, A. Role of Globotriaosylceramide in Physiology and Pathology. *Front. Mol. Biosci.* **2022**, *9*, 20.
- 1278 (41) Batisse, C.; Dransart, E.; Ait Sarkouh, R.; Brulle, L.; Bai, S. K.; Godefroy, S.; Johannes, L.; Schmidt, F. A New Delivery System for Auristatin in STxB-Drug Conjugate Therapy. *Eur. J. Med. Chem.* **2015**, *1281* 95, 483–491.
- 1282 (42) Melendez, A. V.; Velasco Cardenas, R. M.-H.; Lagies, S.; Strietz, J.; Siukstaite, L.; Thomas, O. S.; Tomisch, J.; Weber, W.; Kammerer, B.; Romer, W.; Minguet, S. Novel Lectin - Based Chimeric Antigen Receptors Target Gb3 - Positive Tumour Cells. *Cell. Mol. Life Sci.* **2022**, *79* (10), 1–25.
- 1287 (43) Stargardt, P.; Striedner, G.; Mairhofer, J. Tunable Expression Rate Control of a Growth-Decoupled T7 Expression System by L-Arabinose Only. *Microb. Cell Fact.* **2021**, *20* (1), 1–17.
- 1290 (44) Rosato, F.; Pasupuleti, R.; Tomisch, J.; Meléndez, A. V.; Kolanovic, D.; Makshakova, O. N.; Wiltschi, B.; Römer, W. A Bispecific, Crosslinking Lectinbody Activates Cytotoxic T Cells and Induces Cancer Cell Death. *J. Transl. Med.* **2022**, *20*, 1–26.
- 1294 (45) Galindo Casas, M.; Stargardt, P.; Mairhofer, J.; Wiltschi, B. Decoupling Protein Production from Cell Growth Enhances the Site-Specific Incorporation of Noncanonical Amino Acids in E. Coli. *ACS Synth. Biol.* **2020**, *9* (11), 3052–3066.
- 1298 (46) Abe, A.; Inokuchi, J.-i.; Jimbo, M.; Shimeno, H.; Nagamatsu, A.; Shayman, J. A.; Shukla, G. S.; Radin, N. S. Improved Inhibitors of Glucosylceramide Synthase. *J. Biol. Chem.* **1992**, *267* (2), 191–196.
- 1301 (47) Gallegos, K. M.; Conrady, D. G.; Karve, S. S.; Gunasekera, T. S.; Herr, A. B.; Weiss, A. A. Shiga Toxin Binding to Glycolipids and Glycans. *PLoS One* **2012**, *7* (2), No. e30368.
- 1304 (48) Stargardt, P.; Feuchtenhofer, L.; Cserjan-Puschmann, M.; Striedner, G.; Mairhofer, J. Bacteriophage Inspired Growth-Decoupled Recombinant Protein Production in Escherichia Coli. *ACS Synth. Biol.* **2020**, *9* (6), 1336–1348.
- 1308 (49) Felinger, A.; Pasti, L.; Dondi, F.; Van Hulst, M.; Schoenmakers, P. J.; Martin, M. Stochastic Theory of Size Exclusion Chromatography: Peak Shape Analysis on Single Columns. *Anal. Chem.* **2005**, *77* (10), 3138–3148.
- 1312 (50) Xu, J.; Zhao, W.; Sun, J.; Huang, Y.; Wang, P.; Venkataraman, R.; Yang, D.; Ma, X.; Rana, A.; Li, S. Novel Glucosylceramide Synthase Inhibitor Based Prodrug Copolymer Micelles for Delivery of Anticancer Agents. *J. Controlled Release* **2018**, *288*, 212–226.
- (51) McMillin, D. W.; Delmore, J.; Negri, J. M.; Vanneman, M.; Koyama, S.; Schlossman, R. L.; Munshi, N. C.; Laubach, J.; Richardson, P. G.; Dranoff, G.; Anderson, K. C.; Mitsiades, C. S. Compartment-Specific Bioluminescence Imaging Platform for the High-Throughput Evaluation of Antitumor Immune Function. *Blood* **2012**, *119* (15), 131–138.
- (52) McMillin, D. W.; Delmore, J.; Weisberg, E.; Negri, J. M.; Geer, D. C.; Klippel, S.; Mitsiades, N.; Schlossman, R. L.; Munshi, N. C.; Kung, A. L.; Griffin, J. D.; Richardson, P. G.; Anderson, K. C.; Mitsiades, C. S. Tumor Cell-Specific Bioluminescence Platform to Identify Stroma-Induced Changes to Anticancer Drug Activity. *Nat. Med.* **2010**, *16* (4), 483–489.
- (53) Nudelman, E.; Kannagi, R.; Hakomori, S.; Parsons, M.; Lipinski, M.; Wiels, J.; Fellous, M.; Tursz, T. A Glycolipid Antigen Associated with Burkitt Lymphoma Defined by a Monoclonal Antibody. *Science (80-)*. **1983**, *220* (4596), 509–511.
- (54) Johansson, D.; Kosovac, E.; Moharer, J.; Ljuslinder, I.; Brännström, T.; Johansson, A.; Behnam-Motlagh, P. Expression of Verotoxin-1 Receptor Gb3 in Breast Cancer Tissue and Verotoxin-1 Signal Transduction to Apoptosis. *BMC Cancer* **2009**, *9*, 1–9.
- (55) LaCasse, E. C.; Bray, M. R.; Patterson, B.; Lim, W. M.; Perampalam, S.; Radvanyi, L. G.; Keating, A.; Stewart, A. K.; Buckstein, R.; Sandhu, J. S.; Miller, N.; Banerjee, D.; Singh, D.; Belch, A. R.; Pilarski, L. M.; Gariépy, J. Shiga-like Toxin-1 Receptor on Human Breast Cancer, Lymphoma, and Myeloma and Absence from CD34+ Hematopoietic Stem Cells: Implications for Ex Vivo Tumor Purging and Autologous Stem Cell Transplantation. *Blood* **1999**, *94* (8), 2901–2910.
- (56) Arab, S.; Russel, E.; Chapman, W. B.; Rosen, B.; Lingwood, C. A. Expression of the Verotoxin Receptor Glycolipid, Globotriaosylceramide, in Ovarian Hyperplasias. *Oncol. Res.* **1997**, *9* (10), 553–563.
- (57) Maak, M.; Nitsche, U.; Keller, L.; Wolf, P.; Sarr, M.; Thiebaud, M.; Rosenberg, R.; Langer, R.; Kleeff, J.; Friess, H.; Johannes, L.; Janssen, K. P. Tumor-Specific Targeting of Pancreatic Cancer with Shiga Toxin B-Subunit. *Mol. Cancer Ther.* **2011**, *10* (10), 1918–1928.
- (58) Geyer, P. E.; Maak, M.; Nitsche, U.; Perl, M.; Novotny, A.; Slotta-Huspenina, J.; Dransart, E.; Holtorf, A.; Johannes, L.; Janssen, K. P. Gastric Adenocarcinomas Express the Glycosphingolipid Gb3/CD77: Targeting of Gastric Cancer Cells with Shiga Toxin B-Subunit. *Mol. Cancer Ther.* **2016**, *15* (5), 1008–1017.
- (59) Schubert, T.; Sych, T.; Madl, J.; Xu, M.; Omidvar, R.; Patalag, L. J.; Ries, A.; Kettelhoit, K.; Brandel, A.; Mely, Y.; Steinem, C.; Werz, D. B.; Thuenauer, R.; Römer, W. Differential Recognition of Lipid Domains by Two Gb3-Binding Lectins. *Sci. Rep.* **2020**, *10* (1), 1–12.
- (60) Pellizzari, A.; Pang, H.; Lingwood, C. A. Binding of Verocytotoxin 1 to Its Receptor Is Influenced by Differences in Receptor Fatty Acid Content. *Biochemistry* **1992**, *31* (5), 1363–1370.
- (61) Binnington, B.; Lingwood, D.; Nutikka, A.; Lingwood, C. A. Effect of Globotriaosyl Ceramide Fatty Acid  $\alpha$ -Hydroxylation on the Binding by Verotoxin 1 and Verotoxin 2. *Neurochem. Res.* **2002**, *27* (7–8), 807–813.
- (62) Siukstaite, L.; Imberty, A.; Römer, W. Structural Diversities of Lectins Binding to the Glycosphingolipid Gb3. *Front. Mol. Biosci.* **2021**, *8* (July), 1–16.
- (63) Viel, T.; Dransart, E.; Nemati, F.; Henry, E.; Theze, B.; Decaudin, D.; Lewandowski, D.; Boisgard, R.; Johannes, L.; Tavitian, B. In Vivo Tumor Targeting by the B-Subunit of Shiga Toxin. *Mol. Imaging* **2008**, *7* (6), 239–247.
- (64) Janssen, K.-P.; Vignjevic, D.; Boisgard, R.; Falguières, T.; Bousquet, G.; Decaudin, D.; Dolle, F.; Louvard, D.; Tavitian, B.; Robine, S.; Johannes, L. In Vivo Tumor Targeting Using a Novel Intestinal Pathogen-Based Delivery Approach. *Cancer Res.* **2006**, *66* (14), 7230–7236.
- (65) Mazor, R.; King, E. M.; Pastan, I. Strategies to Reduce the Immunogenicity of Recombinant Immunotoxins. *Am. J. Pathol.* **2018**, *188* (8), 1736–1743.

- 1383 (66) Sandvig, K. NEW EMBO MEMBERS' REVIEW: Entry of Ricin  
1384 and Shiga Toxin into Cells: Molecular Mechanisms and Medical  
1385 Perspectives. *EMBO J.* **2000**, *19* (22), 5943–5950.
- 1386 (67) Sandvig, K. Shiga Toxins. *Toxicon* **2001**, *39* (11), 1629–1635.
- 1387 (68) Vingert, B.; Adotevi, O.; Patin, D.; Jung, S.; Shrikant, P.;  
1388 Freyburger, L.; Eppolito, C.; Sapoznikov, A.; Amessou, M.; Quintin-  
1389 Colonna, F.; Fridman, W. H.; Johannes, L.; Tartour, E. The Shiga  
1390 Toxin B-Subunit Targets Antigen in Vivo to Dendritic Cells and  
1391 Elicits Anti-Tumor Immunity. *Eur. J. Immunol.* **2006**, *36* (5), 1124–  
1392 1135.
- 1393 (69) Center for Drug Evaluation and Research (no date) Guidance  
1394 for industry. *U.S. Food and Drug Administration. FDA.* Available at:  
1395 [https://www.fda.gov/regulatory-information/search-fda-guidance-](https://www.fda.gov/regulatory-information/search-fda-guidance-documents/immunogenicity-testing-therapeutic-protein-products-developing-and-validating-assays-anti-drug)  
1396 [documents/immunogenicity-testing-therapeutic-protein-products-](https://www.fda.gov/regulatory-information/search-fda-guidance-documents/immunogenicity-testing-therapeutic-protein-products-developing-and-validating-assays-anti-drug)  
1397 [developing-and-validating-assays-anti-drug](https://www.fda.gov/regulatory-information/search-fda-guidance-documents/immunogenicity-testing-therapeutic-protein-products-developing-and-validating-assays-anti-drug) (Accessed: March 2,  
1398 2023).
- 1399 (70) Gribben, J. G.; Devereux, S.; Thomas, N. S. B.; Keim, M.;  
1400 Jones, H. M.; Goldstone, A. H.; Linch, D. C. Development of  
1401 antibodies to unprotected glycosylation sites on recombinant human  
1402 GM-CSF. *Lancet.* **1990**, *335* (8687), 434–437.
- 1403 (71) Hwang, W. Y. K.; Foote, J. *Immun. Eng. Antibod. Methods.* **2005**,  
1404 *36* (1), 3–10.
- 1405 (72) Cioci, G.; Mitchell, E. P.; Gautier, C.; Wimmerová, M.;  
1406 Sudakevitz, D.; Pérez, S.; Gilboa-Garber, N.; Imberty, A. Structural  
1407 Basis of Calcium and Galactose Recognition by the Lectin PA-IL of  
1408 *Pseudomonas Aeruginosa*. *FEBS Lett.* **2003**, *555* (2), 297–301.